Bi-monthly • January - February • 2018

ISSN: 0976-2108

BARC NEWSLETTER

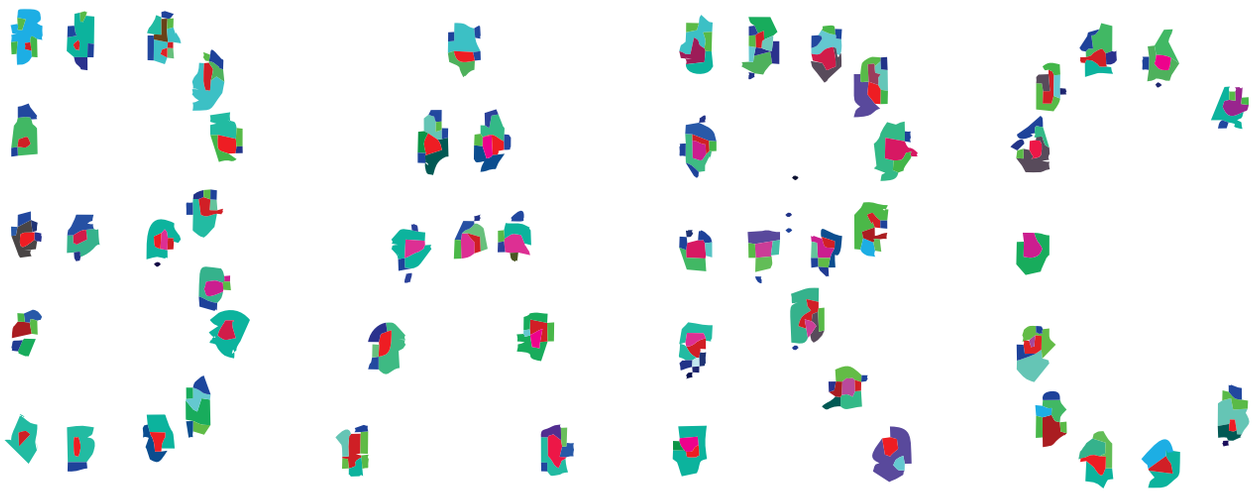

CONTENTS

Development & Demonstration of Hull Batching System for Batching of Metallic De-clad Waste of Fast Reactor Fuel Cycle Facility

Kiran T. Badgujar, S.S. Swain, Arkel Ramesh, Kunjman Singh and K.V. Ravi
Nuclear Recycle Board

Fast Reactor Fuel Cycle Facility (FRFCF) is being constructed at Kalpakkam to close the fuel cycle of Fast Breeder Reactors (FBR). Hull compaction facility is being designed for the first time in India and also planned for the FRFCF. Large volume of hulls will be generated during fuel reprocessing of the FBR spent fuels. Hulls are highly radioactive in nature and require enormous volume for storage thereby imposing burden on the definite storage space available at the Near Surface Storage & Disposal Facility (NSSDF) and Deep Geological Repository. Hulls being hollow cut pieces they provide scope for volumetric reduction thereby minimizing the long term storage space requirements. Conditioning of hulls is planned to be carried out in three stages. In the first stage, entire hull drum containing hulls will be dried to remove the residual water content. This is followed by the second stage which involves hulls contained in a hull drum to be batched into smaller Cans to facilitate the third stage wherein the Cans filled with hulls are compacted in a Hydraulic Super compactor.

A first of its kind prototype of Batching system (1:1 scale) has been developed & demonstrated for batching of Radial subassembly (RSA) and Fuel subassembly (FSA) hulls of FBR. The system has been equipped with remote operability and maintainability features to make it suitable for operation in radioactive hot cells. Electromagnetic vibratory feeder was adopted for hull batching operation. Rigorous batching trials were conducted to generate a baseline data for further active cell operations. The paper describes design philosophy, constructional features, remote handling features & the performance of the batching system during the trials.

Keywords: Radioactive, De-cladding, Vibratory feeder, Hulls, Batching System, Hull Can, FBR, NSSDF

Introduction

The success of the three stage nuclear programme rests not only on the effectiveness of reprocessing & recycling of spent nuclear fuel generated in each stage but also on the safe management of radioactive wastes associated with it. In the chop-leach process of fuel reprocessing, the spent fuel pins are chopped into small pieces for dissolution in nitric acid. The left out empty cylindrical fuel pin cut pieces along with structural material of fuel like spacer wires, fuel end caps & cutting fines obtained after fuel dissolution are referred to as 'Hulls'. They are associated with high level of radioactivity due to residual fission products, alpha contaminants like major & minor actinides and neutron activation products. Current practice of management of hulls is interim storage in the tile holes at NSSDF. These hulls are kept pending for subsequent conditioning before final storage & disposal in Deep Geological Repository. Hulls require enormous volume for storage thereby imposing severe burden on the definite storage space available at NSSDF and Repository. Hulls being hollow cut pieces provide scope for volumetric reduction thereby minimizing the long term storage space requirements at NSSDF & Deep Geological Repository

Volumetric reduction of hulls is planned to be carried out in three stages. In first stage, entire hull drum containing 400-500 litres of hulls will be dried in order to completely remove the residual water content present in the hulls. The second stage involves batching of 400-500 litres of hulls present in the hull drum in to smaller Cans of 60-70 litres capacity. In the third stage, Cans filled with hulls are to be compacted in a 2000Te Hydraulic super compactor [1] to form compacted pucks [2]. The compacted pucks are then loaded in stainless steel canisters and TIG welded before being sent to Alpha Storage Facility (ASF).

Hull batching system (1:1 scale) has been developed & demonstrated at Trombay for batching of RSA & FSA hulls. The system has also been tested for PHWR hulls. The system has been designed with remote operation and maintenance features, which enables the system suitable for radioactive hot cell operations. Fig.1 shows the Batching System installed at Test Facility, Kalpakkam.

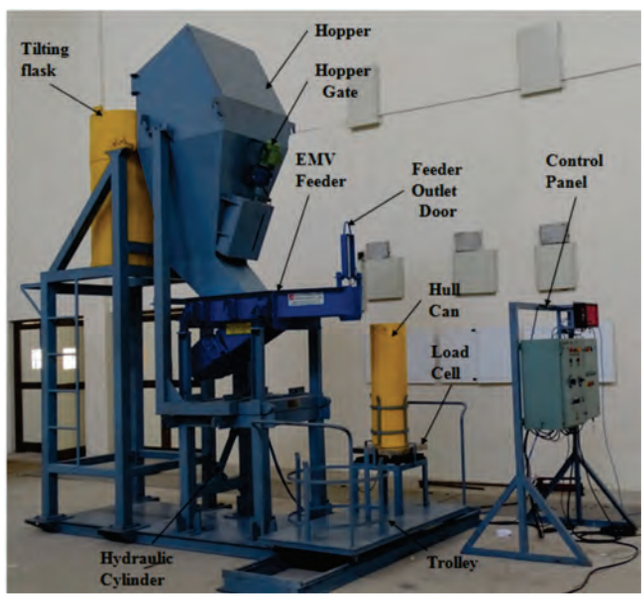

Fig.1: Batching System installed at Test Facility, Kalpakkam

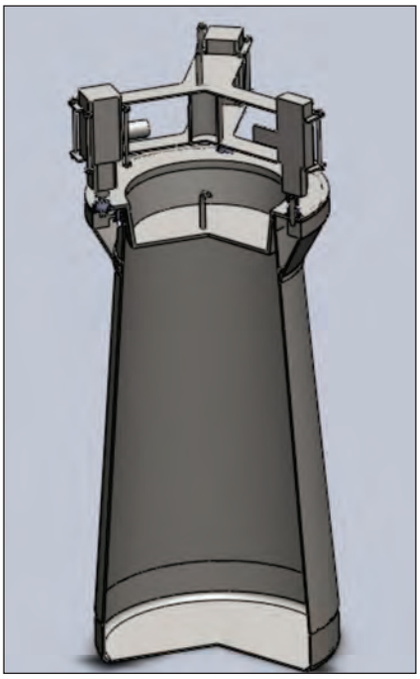

Fig. 2: Schematic of Hull Drum

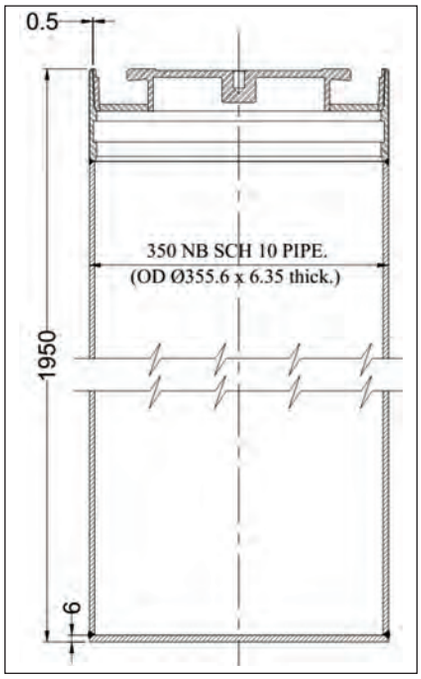

Fig. 3: Hull Puck Canister

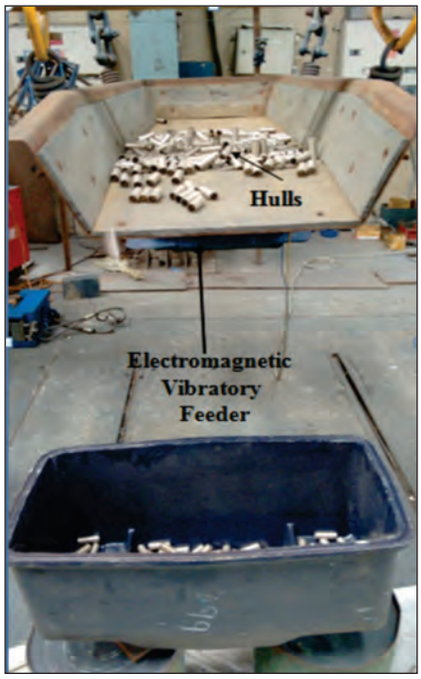

Fig. 4: Mock-up trials on EMV feeder

Development of hull batching system was carried out in several stages. In the first stage, SS hull drum of 700mm Diameter x 1400mm height (schematic shown in Fig. 2) and Hull puck canister of size 350NB x 1950 mm height was designed, developed and tested for remote handling operations (Schematic sketch shown in Fig. 3).

Second stage involved survey of feeders, mock-up trials on various feeders and selection of an appropriate feeder suiting hot cell conditions. Upon testing of various feeders, electromagnetic (EM) vibratory feeder was found most suitable for batching of hulls in the radioactive hot cell. Fig. 4 shows the photograph of mock-up trials on EM vibratory feeder.

Prototype Fast Breeder Reactor employs two types of fuel assemblies i.e. Fuel Sub-Assembly (FSA) & Radial Fuel Sub-Assembly (RSA). Table-1 gives the sizes of PFBR RSA and FSA hulls & their expected generation rate per annum.

System description

Detailed description of individual components of the batching system is as follows:

Hull drum

Development of seal tight hull drum was the first step in the design of batching system in view of alpha content of hulls. Hull drum suiting to both Fuel Reprocessing plant (FRP) as well as Waste Management plant (WMP) has been designed and tested for remote handling operations like handling of lid, empty/filled hull drum with/without lid and hull tilting operations.

Hull drum has been developed along with impact wrench fixture (as shown in Fig.5) for remote locking and unlocking of drum lid.

Table 1: Details of RSA & FSA Hulls

Particulars	FSA	RSA
Material	Stainless Steel D-9	Stainless Steel D-9
Outside Diameter	6.6mm	14.3mm
Thickness	450 μm	900 μm
Length	30-40mm	30-40mm
Hull drum volume (containing 4 batches of fuel reprocessing)	360 litres	400 litres
Annual generation rate (drums/annum)	25 nos.	

Fig. 5: Hull Drum with impact wrench

Tilting flask

It is a cylindrical flask designed to accommodate the hull drum and has provision to tilt the hull drum to 135˚ from vertical position for complete draining of hulls into the Hopper. It has also been provided with an arrester at the top flange to prevent the hull drum from toppling during tilting operation.

Hopper & Hopper Door

Hopper plays a vital role in the optimum performance of the feeder. Parameters governing the hopper design are size of hopper, front wall slope, rear wall slope, throat opening dimensions and gap between hopper & feeder trough. The parameters were arrived at based on the standard practice followed in the industry and repeated trials. The hopper is provided with a motorized fork-type gate (as shown in Fig.6) to control the flow rate of hulls and to reduce the load of hulls on the feeder trough.

Fig. 6: Internal view of fork-type gate HULL DRUM IMPACT WRECH FIXTURE of hull hopper

Electromagnetic Vibratory Feeder (EMV Feeder)

Among various types of feeders available in the industry for conveying bulk solids: Screw conveyers, unbalanced mass motors feeders & EMV feeders were studied and tested. Screw conveyer being susceptible to jamming between conveyor and feeder body owing to the presence of fines & spacer wires along with the hulls was found to be unsuitable for the current application. Unbalanced mass motors type vibratory feeder was also found not suitable due to imprecise control over material flow and higher amplitude of vibrations.

EMV feeder owing to compact construction, amenability for remote operation and maintenance, precise control of flow rate, low amplitude of vibrations, and ability to instantaneous start/stop with an accuracy of one hull and ease in decontamination was found to be suitable for batching operations in hot cell conditions [3]. Specifications of the present EMV feeder are,

- Size of feeder trough: 500 mm width (with tapered discharge) X 1600 mm length X 200 mm height with outlet diameter of 150 mm.
- Conveying Capacity and Power Consumption: 2 Te/Hr, 0.5 kW
- Vibration Frequency & Maximum amplitude of vibration is 3000 VPM & 1.5mm
- Inclination of trough: 0˚
- Mounting of feeder trough: Base mounting with spring damper
- Class of electrical insulation: Class H

Vibratory feeder trough is provided with a pneumatic cylinder operated gate at its outlet to prevent any unintentional material flow during feeding of hulls into the hopper and also during changeover of hull Can after completion of one batch of operation.

Trolley

Trolley is required for positioning of hull Can and hull drum below the outlet of feeder trough. It is also provided with a load cell (300 Kg capacity, ± 50 g accuracy) to measure the weight of hulls filled in the Hull Can. Hull Can (300mm diameter x 1mm thickness x 1000 mm height) was used to collect the hulls from the feeder outlet. It was filled up to height of 900 mm keeping 100mm free board volume to contain the formation of heap. During emergency operation hull drum is positioned below the feeder outlet to collect the residual inventory of hulls.

Control Panel

Control panel controls the operation of vibratory feeder, hopper door, pneumatic operated feeder outlet gate and load cell. Feeder and load cell are equipped with safety interlocks. The feeder operation can be carried out in automatic and as well as manual mode. A selector switch has been provided on the panel to select the type of hull pieces i.e. FSA or RSA to be batched. Set point of load cell was fixed as 80kg for FSA hulls and 78kg for RSA hulls.

Special Design Features

- Since, the batching system has to be operated in a radioactive hot cell, the system was designed to facilitate remote removability of components that may demand maintenance. Components such as hopper, EM vibratory feeder, pneumatic cylinder feeder outlet gate and load cell have been equipped with the remote removability features. Figs. 7, 8, 9 & 10 respectively illustrate the demonstration of remote removability of aforesaid components.
- Electrical insulation of EMV feeder coils are selected as Class-H insulation to have radiation resistance in hot cells.

Fig.7: Remote handling of Hopper

Fig.8: Remote handling of EMV Feeder

Fig. 9: Remote handling of Feeder Gate

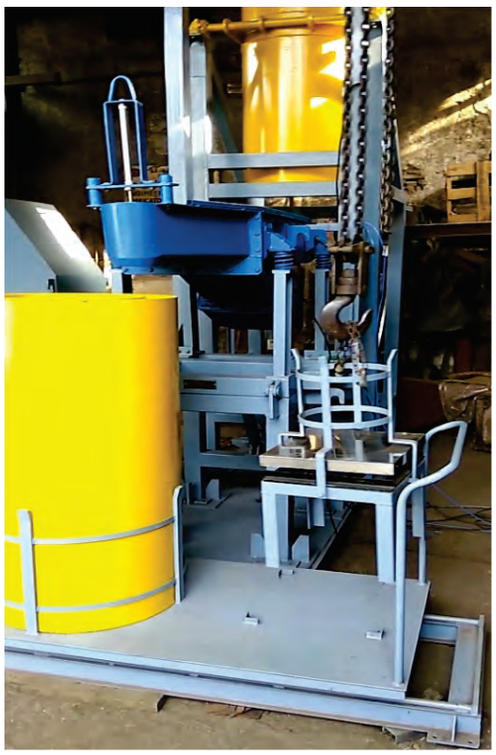

Fig. 10: Remote handling of Load Cell

- Emergency Conditions: In case of failure of EMV feeder, entire hulls residing on the feeder trough and in the hopper can be evacuated by tilting the structure up to 30˚ using hydraulic cylinders. This is possible because of feeder trough & hopper being assembled on a common structural frame, which is in turn hinged to the base structure of batching system. Fig. 11 illustrates the batching system tilted for draining of hulls into the hull drum in the event of emergency.

Fig.11: Emergency Hull Draining operations

Batching trials results and discussions

Batching system was rigorously tested to investigate its performance for RSA and FSA hulls (as shown in Fig. 12 ,13 respectively) under different amplitudes of vibration and to estimate the time taken for batching of hulls from a single hull drum. The base line data generated during the trials would serve as reference for active plant scale operations. Feasibility study for batching of PHWR hulls with 19 pin end plugs was carried out as illustrated in Fig. 14.

Fig.12: Batching of RSA Hulls

Fig.13: Batching of FSA Hulls

Fig. 14: Batching of PHWR Hulls with End plugs

Table 2 & Table 3 respectively show variation in time taken for batching of FSA & RSA hulls for different amplitude of vibration and maximum time taken for complete batching of a hull drum. Fig. 15 and Fig. 16 illustrate the influence of amplitude of vibration on the mass flow rate of hulls and the current drawn for FSA and RSA respectively.

Table 2: Variation in Mass Flow rate of FSA Hulls with Vibration Amplitude

	FSA hulls (6.6mm OD x 0.45mm thk.)			
Vibration amplitude (μm)	Qty.		Time taken (minutes)	Current (A)
	in Kg	in Litres		
375	80	64	7:41	1.7
750	80	64	3.43	2
1125	80	64	2:25	2.5
1500	80	64	1:38	2.6
375	**450**	**360**	**43**	**1.7**

Table 3: Variation in Mass Flow rate of RSA Hulls with Vibration Amplitude

	RSA hulls (14.3mm OD x 0.9mm thk.)			
Vibration amplitude (μm)	Qty.		Time taken (minutes)	Current (A)
	in Kg	in Litres		
375	78	64	5.17	1.6
750	78	64	3.40	1.8
1125	78	64	2.08	1.9
1500	78	64	1.39	2.5
375	**488**	**400**	**33**	**1.6**

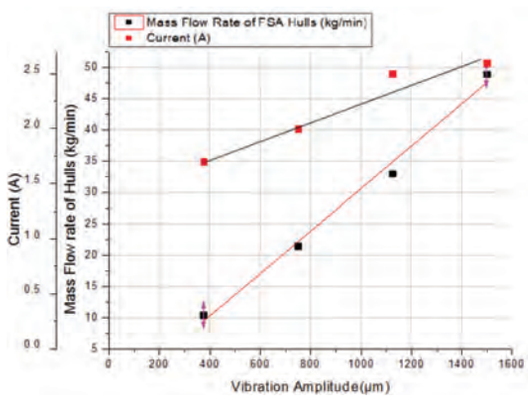

Fig. 15 Variation of Mass Flow rate & Current with amplitude of vibration for FSA hulls

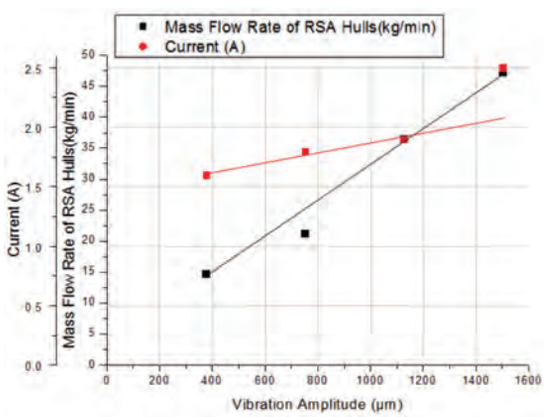

Fig. 16: Variation of Mass Flow rate & Current with amplitude of vibration for RSA hulls

It was observed that the mass flow rate of hulls increased with an increase in the vibration amplitude. Total time taken for complete batching of a hull drum was determined to be 43 minutes and 33 minutes for FSA and RSA hulls respectively. Low mass flow rate of FSA hulls is attributed to higher flow resistance (interlocking) of FSA hulls due to their smaller size compared to RSA hulls.

The hull tilting operation ensured complete draining of hulls from hull drum in to the hopper. The EMV feeder control during instantaneous start/stop condition was to the extent of control of one hull thereby rendering precise control over the flow rate of hulls. Remote removability of individual components such as hopper, feeder, feeder outlet door and load cell was demonstrated. Tilting of hopper and feeder assembly by means of hydraulic cylinders to completely drain out the residual hulls under emergency conditions, was also demonstrated.

Summary

The batching trials and demonstration of remote removability features establish the suitability of the batching system for active plant operations. The optimum operating parameter for batching of FSA hulls shall be 80kg/ Can with a cycle time of 7.41minutes for a vibration amplitude of 375μm, and for RSA hulls it shall be 78kg/Can & cycle time of 5.17minutes for 375μm vibration amplitude. The current batching system with certain modifications can be directly adopted for active plant scale operations. Modifications include: housing the system in an enclosure maintained at a negative pressure to prevent any contamination spread, the tilting flask housing hull drum can be motorized with provision for tilting by means of in-cell crane in the event of emergency and the trolley meant for positioning of hull Can and hull drum for the receipt of hulls, can be motorized with a manual override feature. The current batching system can also be employed for batching of PHWR hulls with 19 pin end plugs by eliminating the hopper door.

Acknowledgements

Authors are extremely grateful to Shri H R Pimparkar, GM, KNRPD & NRPSED, NRB and Shri A.A. Manole, SO/G, NRB for their invaluable guidance. The authors are thankful to Shri R. Srinath, SO/D, NRB, Shri B. S. Jatav, TO/D, NRB for their contribution during the course of inspection, testing and trials. The authors are also thankful to Shri B. K.Singh, SO/F, KNRPC/ NRB, Shri Sunil Kumar Verma, SO/E, IGCAR & Shri Prasath S, SA/C, IGCAR for their contribution during installation & commissioning at the test facility.

References

1. A.A. Manole, P.P. Karkhanis, Kailash Agarwal, Shekhar Basu, "Development of Hull Compaction System for Nuclear Recycle Facility", (BARC Newsletter), Issue no. 334, (2013): 32-37
2. F. Chotin, Ph. Pinson, COGEMA, "The Atelier De Compactage Des Coques (ACC) Facility: The R&D Programme", IAEA-SM-357/30
3. Zeljko V. Despotovic, Milan Lecic et al. "Vibration Control of Resonant Vibratory Feeders with Electromagnetic Excitation, FME Transactions", Vol.42, No. 4, (2014)

Development of Position Sensitive Multi-wire Gas Detectors for Nuclear Physics Experiments

D.C. Biswas, R.P. Vind, Nishant Kumar, R.V. Jangale, A.L. Inkar and Y.K. Gupta
Nuclear Physics Division
A.T. Chaudhari, L.S. Choughule and Manish Kumar
Technical Physics Division

Over the last few decades, a variety of gas detectors have been developed in BARC for use in heavy-ion induced nuclear physics experiments at Pelletron-LINAC Facility (PLF). Here we discuss about our recent accomplishment in the development of two-dimensional position sensitive multi-wire gas detectors. The position measurement has been carried out by employing delay-line read out method and the resolution is about 1.0 mm both in X and Y directions. The velocity of the fission fragments (FFs) are measured by employing time of flight (TOF) methods. Fission fragment mass distributions have been measured by employing two similar Multi-wire Proportional Counters (MWPCs). These indigenously developed detectors are the key instruments for carrying out experiments to investigate fission dynamics in heavy-ion induced reactions.

Introduction

Historically gas detectors were the first electrical devices, developed for the use in nuclear physics experiments as radiation detectors. They are economical, simple to operate and incur low maintenance cost. These detectors exhibit several advantages over the existing solid state and scintillation detectors in respect of versatility of construction, large area coverage, immunity to radiation damage and pulse height defect etc. Moreover, the flexibility in changing the detector thickness by varying the gas pressure is very useful to detect different charged particles produced in nuclear reactions.

In BARC, the nuclear physics research using gas detectors started in 1960's with the development of a Twin gas ionization chamber for the detection of Fission Fragments (FFs) produced by using thermal neutrons from APSARA and CIRUS reactor facilities. This detector has been used extensively in several experiments for the understanding of nuclear fission process from the coincidence measurement of both the fragments along with neutrons, light charged particles, X-rays and gamma rays [1-4]. In mid-eighties, there had been renewed interest in the development of gas detectors for the utilization of heavy-ion beams from Pelletron LINAC facility PLF, BARC-TIFR. Different types of hybrid detector telescopes, position sensitive gas ionization chambers were developed in various configurations for the detection of fission fragments and projectile-like particles [5-9]. These detectors are used in studying heavy-ion reaction mechanism and fission process by measuring the mass, charge, kinetic energy and angular distributions of heavy ion reaction products [10-16].

In comparison to the ionization chambers, the gas proportional counters provide fast timing signals and are found to be suitable in high counting experiments. Since the invention of the MWPC (Multi-Wire Proportional Counters) by Charpak et al. [17], these detectors are extensively used in high energy physics experiments for particle localization. The MWPC detector has very good timing characteristics and is commonly used for the velocity measurement. Because of the good position resolution and detector efficiency, position sensitive multi-wire proportional detectors have also been used for nuclear physics experiments in different sizes and geometries, in particular for heavy ion induced fission reaction studies. In these experiments, the velocity of the fission fragments are determined by combining accurate measurement of the path length and the time of flight (TOF) by using two MWPC detectors.

The precise measurement of the fragment velocities are very crucial for obtaining the mass distribution of FFs. The accuracy of the time intervals of the signals in a pair of detectors separated by flight distances is important for the velocity measurement, and the uncertainty in the time measurement can be minimized by using two detectors having fast timing response. The mass measurement by employing the TOF technique using MWPC is more accurate in contrast to the double energy (2E) measurement by using ionization chamber or semiconductor detectors. The mass distribution is broadened significantly due to the emission of prompt neutrons in case of the double energy measurements, whereas it is less influenced for double velocity (2v) measurements. Therefore, the overall mass resolution in 2v method is better than the double energy measurements.

Development of multi-wire cathode strip detector (MCSD)

A gas filled bi-dimensional MCSD has been developed for the detection of fission fragments (FFs). The main body of the MCSD mounted inside a bell-jar setup is shown in Fig. 1. The detector has three electrode planes consisting of cathode strips, anode wires and split-cathode wires. More details of the construction of the detector and the performance characteristics have been reported earlier [18]. High impedance discrete delay line (developed in BARC) read out method [19] was employed for extracting position information in X and Y-directions.

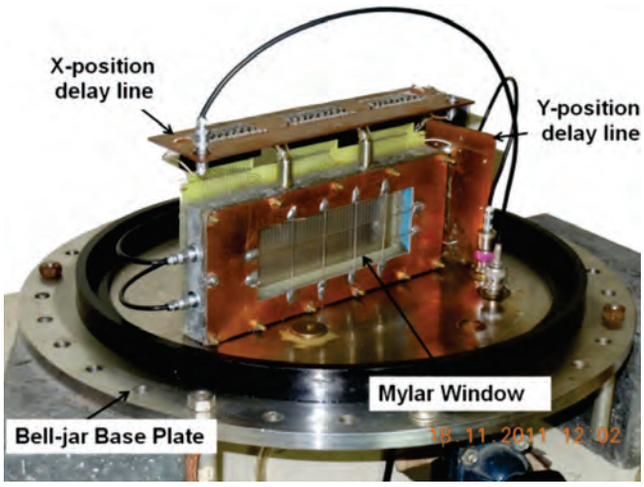

Fig.1: Experimental setup showing bi-dimensional MCSD for testing with ^{252}Cf source

The MCSD has been used in various experiments in PLF for the measurement of FFs produced in heavy-ion reactions. In these reactions, various projectile-like fragments (PLFs) are produced in addition to the FFs. We have operated the detector with P-10 gas (90% Ar + 10 % CH_4) at a pressure of 15 Torr and the energy loss of the PFs is very small in comparison to the FFs. Thus, the PFs provide negligible signal and only the FFs are detected in the MCSD [18]. The rise time of the anode, X and Y signals were ~ 20 ns after shaping by using timing filter amplifiers. The maximum pulse heights of the signals were ~ 100 mV, after the amplification by fast amplifier (without using any Timing Filter Amplifier). Since the pulse height of the signals from MCSD were relatively small, it was not efficient enough to detect the fission fragments of lower energies.

Development of Multi-wire gas Proportional Counters (MWPC)

As the signals from MCSD are slow, these detectors are not suitable for mass distribution measurements using time of flight (TOF) method. We have developed two large area (17.5 cm × 7.0 cm) position sensitive Multi-Wire Proportional Counters (MWPCs) for the measurement of fission fragment mass distribution using heavy ion beams at Pelletron-LINAC facility, TIFR. The detectors were characterized using FFs from ^{252}Cf source to obtain position information by employing delay-line read out method.

The MWPC consists of total five wire planes. It has one anode (A) wire plane, two sense wire planes (X and Y) for position information and two cathode (C) wire planes. The schematic sketch of the cathode, anode, X and Y sense wire planes, along with their geometric separations are shown in Fig.2. The separation between the anode wire plane and X (or Y) planes are 2 mm, while the separation between X (or Y) and the cathode plane is 4.8 mm. The wires were fixed on PCB board of thickness 1.6 mm. The main body of the MWPC is made of aluminum to mount all the wire planes inside it. The mounting arrangement of the wire planes and the electronic connectors inside the detector main body is shown in Fig.3.

Each wire is essentially independent and behaves like a proportional counter. The anode plane consists of gold plated tungsten (Au-W) wires having 10 μm diameter and the separation between two adjacent wires is 2 mm. Both the cathode, X and Y sense wire planes were also made of Au-W wires having 50 μm diameter and are fixed at a separation of 2 mm. The orientation of the X and Y sense wire planes are orthogonal to each other.

A Stretched Mylar foil of thickness ~ 1 μm and of size 17.5 cm × 7.0 cm was used as entrance window of the detector. The window foil was supported by stainless steel wires of diameter 0.5 mm by fixing on a PCB frame at a separation of 10 mm in both X as well as Y directions. Two gas feed-throughs were connected to the detector for operating the MWPC in gas-flow mode. The flow of the gas was maintained at a constant low pressure (2-3 Torr) by using an automatically controlled gas-flow system supplied by M/s Alpha Pneumatics, Thane, India.

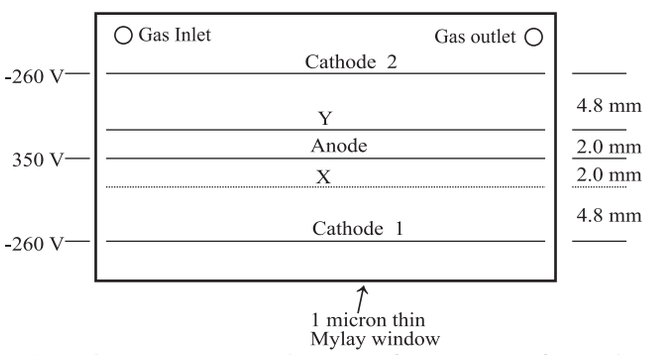

Fig. 2: Schematic drawing of the vertical cross-sectional view of MWPC showing 5 wire planes. The separation and typical voltages applied to the cathodes and anode are also shown in the figure

The X-sense wire plane has 100 wires with a pitch of 2 mm, while 40 wires of 2 mm pitch are used for Y-sense wires. We have employed the delay-line read out method for deriving X and Y position information of the detector. The delay between the successive X-sense wires is 2 ns, while that between the Y-sense wire is 5 ns. Using the anode signal as "Start" and X-signal as "Stop", the time difference between these two signals gives the X-position of the detector. Similarly, the time difference between the anode and Y-signal defines the Y-position.

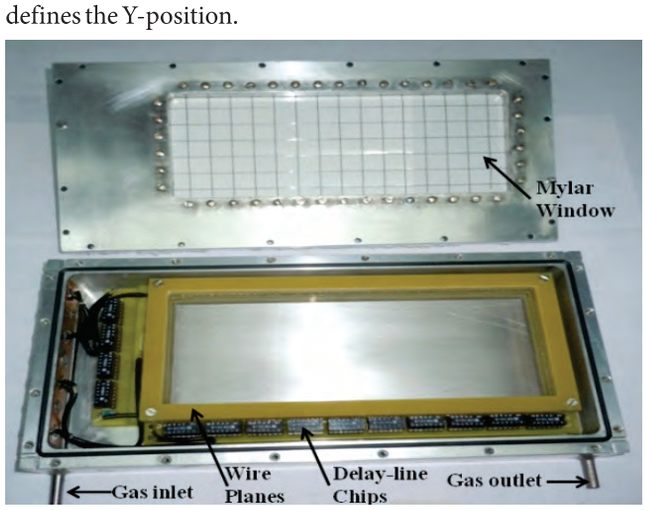

Fig. 3: Mounting arrangement of the anode, 2 cathodes, X and Y sense wire planes of the MWPC inside an aluminum chamber.

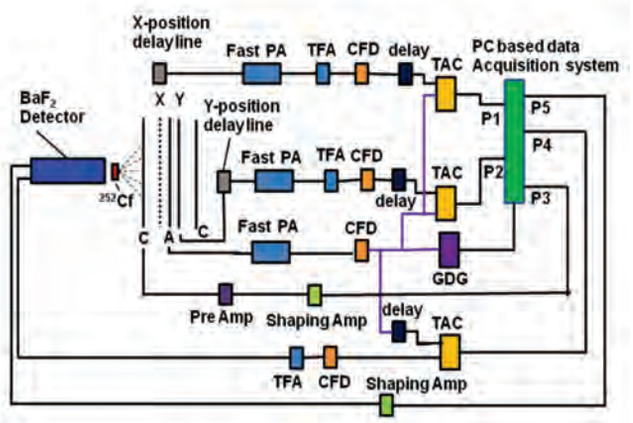

Fig. 4: Electronic block diagram of the setup used for the TOF measurement

The detector was tested with FFs from ^{252}Cf source for the uniformity of the position readouts, and also for checking the correlation between the timing of anode pulse and position (X,Y) delay-line signals. Fig. 4 shows the schematic block diagram of the electronic setup along with the data acquisition system. The anode and the cathode wire planes were biased at +350 V and -260 V respectively, whereas the X and Y sense wire planes were not given any bias voltage and grounded through delay-lines. The MWPC detector has been operated with isobutene gas at a pressure of 3 Torr. The E/p ratio, where E is the electric field between the cathode and anode wire planes, and p is the gas pressure, was high enough (~ 300 V cm^{-1} Torr^{-1}) to produce secondary multiplication of the primary electrons produced in the region between the cathodes and the sense wires. The secondary electrons enter the region between the sense wires and the anode. Due to the large electric field near the anode wires, it causes a localized avalanche of electrons and ions in the vicinity of the anode, which produces a fast rising negative pulse at the anode and positive signals at the sense wires.

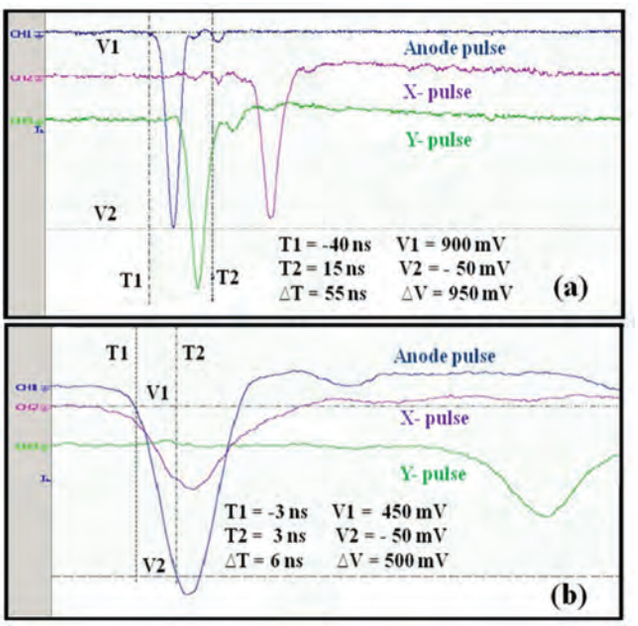

Fig. 5: (a) Pulses taken by a digital oscilloscope from the fast pre-amplifier of the anode, X and Y planes after shaping with suitable integration and differentiation using TFA. (b) Pulse shapes of the signals immediately after the fast pre-amplifier.

A wide band fast timing pre-amplifier (Fast PA) was used to amplify the negative anode pulses. The X and Y sense wire signals have positive polarity and were also amplified by two fast timing pre-amplifiers. We have measured the rise time of the signals with and without the timing filter amplifiers (TFA) as shown in Fig. 5(a) and (b) respectively. The rise time of the anode, X and Y signals were ~ 6 ns immediately after the fast amplifier and is about ~ 9 ns after the TFA, using suitable integration and differentiation time of about 10-20 ns.

The TOF measurements were carried out using a BaF_2 scintillator and a MWPC detector. The schematic diagram of the experimental set up is shown in Fig. 6. A ^{252}Cf source was mounted on a flange inside a scattering chamber, which was evacuated to a vacuum of 10-3 Torr. For the detection of FFs, the MWPC detector was mounted on a platform inside the vacuum chamber at 54.5 cm and 85.5 cm from the source in two different measurements. The BaF_2 detector was mounted outside the flange of the vacuum chamber at a distance of 1.0 cm from the source. In spontaneous fission of ^{252}Cf, about 10 prompt γ-rays are also emitted along with the FFs. The gamma rays are detected by the BaF_2 detector, which gives a fast signal and was used as "Start signal" for the TOF experiment. After traveling the flight path in vacuum, the fission fragments reach the MWPC and lose energy in the gaseous medium. It gives a fast timing signal from the anode that was used as "Stop signal" in the experiment.

Timing characteristics of the signals from MWPC

The detector was tested in the laboratory with ^{252}Cf source for the uniformity of the position readouts, and also for checking correlation between the timing of anode pulse and position (X,Y) delay-line signals. The anode and the cathode wire planes were biased at +350 V and -260 V respectively, whereas the X and Y sense wire planes were not given any bias voltage and were grounded through delay-lines. The MWPC detector has been operated with isobutene gas at a pressure of 3 Torr. The E-p ratio, was high enough (~ 300 V cm^{-1} Torr^{-1}) to produce secondary multiplication of the primary electrons produced in the region between the cathodes and the sense wires. The secondary electrons enter the region between the sense wires and the anode. Due to the large electric field near the anode wires, it causes a localized avalanche of electrons and ions in the vicinity of the anode, which produces a fast rising negative pulse at the anode and positive signals at the sense wires.

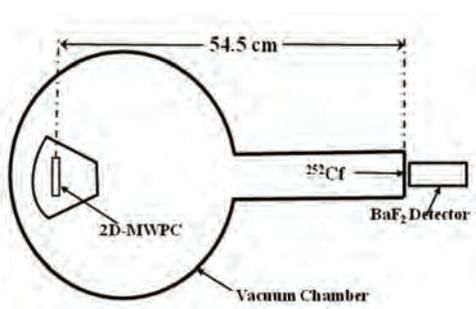

Fig. 6: Schematic diagram for TOF measurement setup

A wide band ORTEC VT120A type fast timing pre-amplifier (Fast PA) was used to amplify the negative anode pulses. The X and Y sense wire signals have positive polarity and were amplified by two ORTEC VT120B type fast timing pre-amplifiers.

Typical anode pulses from VT120A pre-amplifier with ^{252}Cf source were 500 mV for FFs and less than 5 mV for alpha particles. Since the anode signal is primarily used for the timing measurements of fission fragments, its output from fast pre-amplifier is directly fed to Constant Fraction Discriminator (CFD) for further processing. The timing outputs of the sense wire signals (X and Y) were about 150 mV, which were filtered through timing filter amplifiers (TFAs) and fed to CFD. After the TFA, the pulse height of the signals were about 950 mV. The output signal of the anode CFD becomes the "Start" pulse for two Time-to-Amplitude Converters (TACs) that are used for X and Y position measurements. It was also used for generating master gate pulse through a gate & delay generator (GDG). The output of the CFDs of the X and Y sense wires are suitably delayed and used as "Stop" pulses for obtaining position information from the corresponding TAC modules. The output pulse heights of both the TAC's are proportional to the delay between the anode and sense wire signals, which translate the position information of the detector in two dimensions.

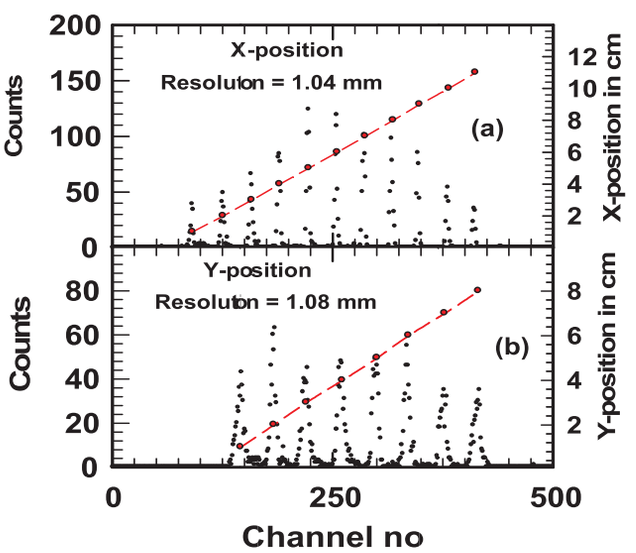

Fig. 7: Position spectrum both in X and Y directions

The linearity of the position signal has been checked by putting a mask on the face of the detector. There were 11 opening holes in X direction of the mask with 1.0 mm diameter and the separation between the center of the two adjacent holes was 10 mm. In the Y-direction, 8 opening holes of 1.0 mm diameter, with a separation of 5 mm were used. The peaks corresponding to X and Y directions are shown in Fig. 7. The mean peak position and width have been obtained by fitting the distribution with Gaussian function. The peak channel number corresponding to the center of each opening hole, has been plotted as a function of hole position (in mm), also shown in the same figure (right Y-axis). The error in the Gaussian fitting of the intensity profile and hence in the position measurement is within the size of the circle. It is observed that the position peak channels show linear behavior with the peak position. The position resolution (FWHM) both in X and Y directions are obtained from the fitting of the peaks and are found to be about 1.04 ± 0.03mm and 1.06 ± 0.04 mm respectively.

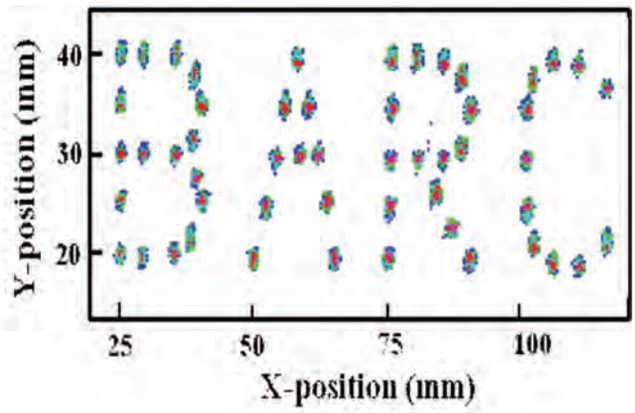

Fig. 8: Two dimensional spectrum of coordinates X and Y obtained by keeping a mask with acronym ``BARC" having 1 mm diameter holes and placing in front of the detector

The position sensitivity of the detector in two dimensions has been tested with FFs from ^{252}Cf fission source and by putting a mask of "BARC" (acronym of Bhabha Atomic Research Centre) in front of the detector. Each alphabet of the mask "BARC" was realized in a dot matrix format by drilling small holes of 1.0 mm diameter. The center to center distance of the holes for straight portion of each alphabet is 5 mm and for the curved portions it is 2.5 mm. The 2-D position spectrum as shown in Fig. 8, gives a clear image of the acronym "BARC", demonstrating very good performance of the detector for position measurement in two dimensions.

Timing characteristics of the BaF_2 detector for gamma rays

A BaF_2 detector of length 2.5 cm was used in the present experiment. It is of conical shape geometry, having 2.5 cm diameter in the front and 3.8 cm in the back face, which is coupled with a photomultiplier tube. The light output pulse from the de-excitation of BaF_2 has two components: one with a decay time of 630 ns and an other with a decay time of 0.6 ns. The fast component only accounts for 20% of the total light output of BaF_2, the remaining 80% is made up by the slow component. The time resolution of the BaF_2 detector has been obtained by using two identical detectors and measuring the two coincidence gamma rays of energies 1.173 and 1.332 MeV, emitted from a ^{60}Co source. Positive bias voltages (+1700 V) were applied in both the detectors using two independent HV supplies. The energy of the gamma rays was measured by amplifying the signal using a shaping amplifier. The output pulses from the BaF_2 detectors were found to be sharp, in having rise time of ~ 3.2 ns and amplitude of around 500 mV. The pulse was directly fed to CFD without any shaping and amplification. The output pulse from the CFD of one BaF_2 was fed to the "Start" of the TAC and the pulse from the CFD of other BaF_2 was delayed through a delay box and eventually given to the "Stop" of the TAC. The time resolution (FWHM) obtained for the BaF_2-BaF_2 detector system in this experiment is about 233 ± 6 ps.

Measurement of the TOF and velocity distribution for fission fragments from ^{252}Cf

For the TOF measurement, one of the MWPCs is mounted inside a scattering chamber on a rotatable arm of the chamber with one of its ports extending outside the chamber and the fission source (^{252}Cf) is mounted on its flange from inside (see Fig.6). A BaF_2 scintillation detector placed outside of the flange that detects the prompt gamma rays emitted from the fission fragments. Fig. 6 depicts the schematic diagram of TOF setup. The path length from fission source to MWPC is 54.5 cm. and the experiment has been repeated for 85.5 cm path length of the fission fragments.

The prompt gamma rays emitted from the fission fragments were measured by using a BaF_2 scintillation detector in coincidence with the signals from the MWPC. The TAC spectrum was obtained by using the "Start signal" from the BaF_2

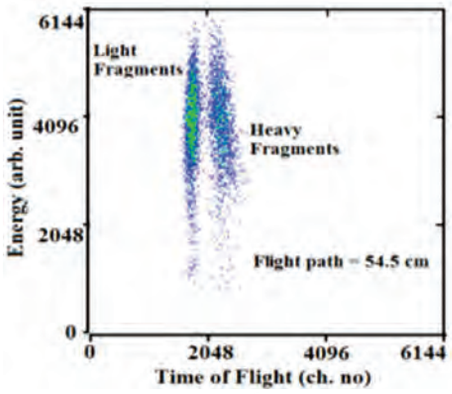

Fig. 9: Two dimensional plot of TOF vs energy, showing clear separation for light and heavy fission fragment groups produced from ^{252}Cf.

and "Stop signal" from the anode of the MWPC detector. The measurement was repeated by extending the flight path to 85.5 cm, using a stainless steel tube of known length of 31 cm. From the known path length and measured TOF, the velocity was obtained after processing the event by event LIST mode data and calculating the flight path by using the following equations:

$$D = (x^2 + y^2 + d^2)^{½} \quad \text{and} \quad v = D\ (cm)/t\ (ns)$$

Where, the flight path (D) of the fission fragments are calculated from the known distance of the MWPC center point (d) from the ^{252}Cf source and the position co-ordinates (x,y) in the MWPC. Here 'v' is the velocity and 't' is the TOF of the fragments.

The energy signals from the cathodes were amplified by a charge sensitive preamplifier (PA) followed by shaping amplifier. Fig. 9 shows the 2D-plot of TOF versus Energy of the fission fragments for the flight path of 54.5 cm. It is observed in the 2D spectrum, both the fission fragment groups are clearly separated as the lighter fragments move faster than the heavier ones. The TOF distribution spectra obtained for both the distances are shown in Fig. 10. By using double Gaussian fit to the timing spectrum, we have obtained the width of the TOF distribution. It is observed that the time spread is large for the heavy fragments as compared to the light fragments due to the velocity dispersion. We have also plotted the velocity distribution data in Fig. 10 and the measurements are found to be consistent for both the distances. The mean of the most probable velocities (V_L and V_H respectively refer to light and heavy fragments) measured for both the distances are V_H = 1.035 ± 0.003 cm/ns and V_L = 1.378 ± 0.004 cm/ns respectively.

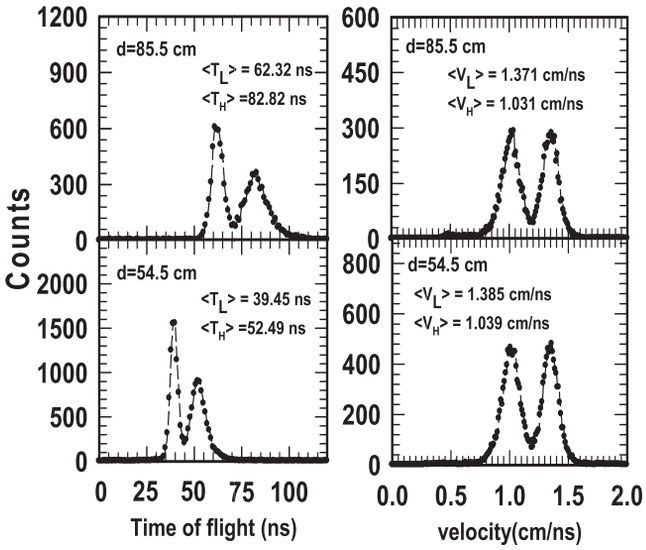

Fig. 10: TOF and velocity spectra of fission fragments for d = 54.5 and 85.5 cm.

Measurement of the mass distribution of the fission fragments in heavy-ion reaction

For the measurement of FFs mass distribution employing the double velocity (2*v*) method, two identical MWPC detectors were used in an in-beam experiment at BARC-TIFR Pelletron-LINAC accelerator facility, Mumbai. Pulsed beam of ^{28}Si having 154.6 MeV energy with ~1.5 ns width and a period of 107.3 ns was used in this measurement. The Fission fragments produced in ^{28}Si + ^{197}Au reaction, were detected in coincidence by using two position-sensitive MWPC detectors mounted inside the general purpose scattering chamber of diameter 1.5 meter, on two movable arms as shown in Fig. 11. The anode plane was normal to the particle trajectories passing though the center of the detectors.

The target was ~ 250 μg/cm^2 self supporting gold foil. One of the detector was placed at a distance of 55.0 cm (MWPC1) from the target ladder, while the other at a distance of 27.5 cm

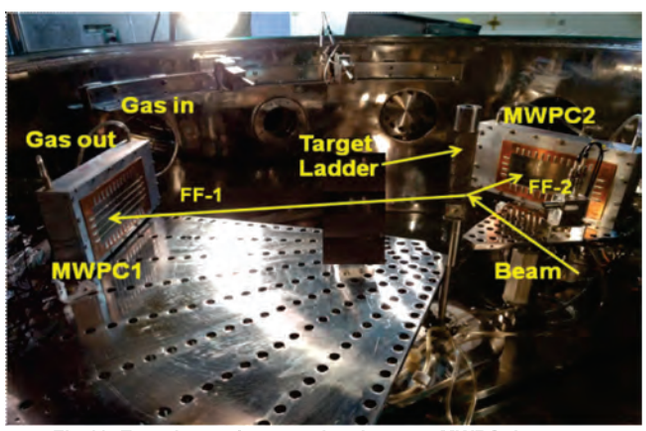

Fig.11: Experimental setup showing two MWPC detectors mounted inside a general purpose scattering chamber at Pelletron-LINAC facility

(MWPC2) and the angular coverage of the detectors were around 18° and 35.3° respectively. The folding angle for ^{28}Si + 197Au reaction at a beam energy of 154.6 MeV is 144° and the detectors were mounted at $\theta_1 = 72°$ and $\theta_2 = -72°$.

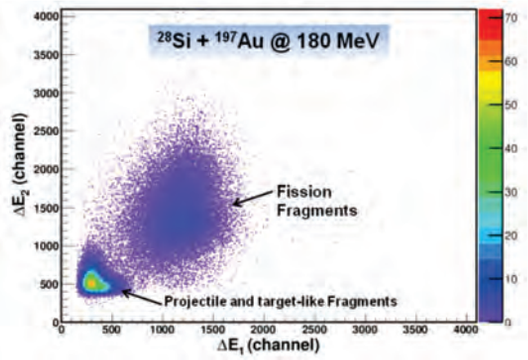

Fig. 12: Separation of fission fragments from projectile-like fragments from the 2D plot of energy loss, ΔE1 and ΔE2 in MWPC1 and MWPC2 respectively

Isobutene gas at a pressure of 3.0 Torr was used inside the MWPCs for the detection of fission fragments. The X,Y positions, the energy loss in each of the detectors, the time difference between the arrivals of coincident fragments at the detectors and individual time of flight of the fragments with respect to RF beam bunching signal were recorded event by event. The position calibration of the detectors were carried out using the known positions of the edges of the detectors, when the events were collected in singles mode using ^{252}Cf source.

The velocities were reconstructed from the timing and position information obtained in X and Y directions. To obtain mass distribution, the conservation of momentum was used and the velocities were transformed to center of mass frame. The mass distribution for ^{28}Si + ^{197}Au reaction has been obtained from the measurement of the TOF of the correlated fragments by both the MWPCs. From two dimension plot of ΔE1 (energy loss in MWPC1) and ΔE_2 (energy loss in MWPC2) as shown in Fig. 12, it is clearly seen that the FFs are separated from the projectile-like fragments. The analysis procedure for obtaining velocity distribution and fission fragment mass distribution from the measurement of TOF, has been discussed in a recent publication [20].

Summary and Conclusions

In summary, we have developed two different types of multi-wire gas proportional detectors viz. MCSD and MWPC for the detection of FFs produced in nuclear fission. These detectors were characterized in the laboratory using ^{252}Cf spontaneous fission source. The anode pulses from the MWPC is very fast (rise time ~ 6 ns). The position information has been obtained by using the delay-line method and the resolution is about 1.0 mm in both X and Y directions for MWPC. The velocity distribution of fission fragments produced in spontaneous fission of ^{252}Cf source has been measured by TOF method using a BaF_2 detector as "Start" and MWPC as "Stop" detector. Two similar MWPCs were used for studying the FFs mass distribution in heavy ion induced reactions, from the simultaneous measurement of the velocity distribution of the fragments simultaneously.

Acknowledgements:

Authors acknowledge Dr. B.V. John, Dr. B.N. Joshi and G.K. Prajapati for their fruitful discussions on this work. We are grateful to the staff of MDPDS, BARC workshop for the design & fabrication of the mechanical structure of the MWPCs. We are also thankful to the Pelletron-LINAC accelerator operating staff for facilitating smooth separation of the machine during the experiment.

References:

1. S.S. Kapoor, R. Ramanna, Phys. Rev. 133 (1964) 598.
2. S.S. Kapoor, R. Ramanna, P.N. Ramarao, Phys. Rev. 131 (1963) 283.
3. R. Govil, S.S. Kapoor, D.M. Nadkarni, S.R.S. Murthy, P.N. Ramarao, Nucl. Phys. A410 458 (1983).
4. M.S. Samant, R.P. Anand, R.K. Choudhury, S.S. Kapoor, D.M. Nadkarni, Phys. Rev. C51 3127 (1995)
5. M.N. Rao, D.C. Biswas and R.K. Choudhury, Nucl. Instr. & Meth. B51 (1990) 102.
6. D.C. Biswas, M.N. Rao and R.K. Choudhury, Nucl. Instr. & Meth. B53 (1991) 251.
7. D.C. Biswas, V.S. Ambekar, L.M. Pant, B.V. Dinesh, R.K. Choudhury, Nucl. Instr. & Meth. A 340 (1994) 551-554.
8. B.V. Dinesh, R.G. Thomas, B.K. Nayak, D.C. Biswas, A. Saxena, L.M. Pant, P. K. Sahu, and R. K. Choudhury, Nucl. Instr. & Meth. A452 (2000) 338.
9. L.M. Pant, D.C. Biswas, B.V. Dinesh, R.G. Thomas, A. Saxena, Y.S. Sawant, R.K. Choudhury, Nucl. Instr. & Meth. A 495 (2002) 121–131.
10. D. C. Biswas, R. K. Choudhury, B. K. Nayak, and D. M. Nadkarni, V. S. Ramamurthy , Phys Rev C 56 (1997) 1926.
11. A. Chatterjee, A. Navin, S. Kailas, P. Singh, D.C. Biswas, A. Karnik, and S.S. Kapoor, Phys Rev C 52, 3167 (1995).
12. Y.S.Sawant, A. Saxena, R.K. Choudhury, P.K. Sahu, R.G. Thomas, L.M. Pant, B.K. Nayak, D.C. Biswas, Phys Rev C 70, 051602(R) (2004).
13. L.M. Pant, R.K. Choudhury, A. Saxena, and D.C. Biswas, Eur. Phys. J. A 11, 47–58 (2001).
14. Y. K. Gupta et. al, Phys. Rev. C 84, 031603® (2011).
15. Y. K. Gupta, D. C. Biswas, Bency John, B. K. Nayak, A. Chatterjee, and R. K. Choudhury, Phys. Rev. C 86, 014615 (2012).
16. D.C. Biswas and R.K. Choudhury, BARC News letter, Founder's day special issue, Oct 2000 No. 201.
17. G. Charpak, R. Bouclier, T. Bressani, J. Favier and C. Zupancic, Nucl. Instr. & Meth. 62 (1968) 262.
18. R. P. Vind, D. C. Biswas, Y. K. Gupta, A. L. Inkar, R. V. Jangale, G. K. Prajapati, B. N. Joshi, B. V. John, B. K. Nayak, and R. K. Choudhury, IEEE Trans. Nucl. Sci. Vol 60 No 6 (2013) 4650.
19. R.P. Vind, A.L. Inkar, R.K. Choudhury, B.K. Nayak, A. Saxena, R.G. Thomas, D.C. Biswas, B.V. John, Nucl. Instr. & Meth. A 580 (2007) 1435–1440.
20. D. C. Biswas, R. P. Vind, Nishant Kumar, Y. K. Gupta, A. L. Inkar, R. V. Jangale, G. K. Prajapati, B. N. Joshi, S. Mukhopadhyay, Shradha Dubey, Nucl. Instr. & Meth. A 901 (2018) 76.

Development of Diamond like Carbon-SiOx (DLC-SiOx) as Anti-Corrosive and Oxidation Resistant Coating for Application in Compact High Temperature Reactor (CHTR)

N. Chand, R. Kar, A. Bute and S.Sinha
Laser & Plasma Surface Processing Section
S.P. Chakraborty
Materials Science Division

Plasma enhanced chemical vapour deposition (PECVD) is one of the most favourable tools for deposition of different types of thin films. We have used this technique to deposit diamond like carbon - SiOx (DLC-SiOx) coating on Titanium Zirconium Molybdenum (TZM) alloy which is a design material for compact high temperature reactor (CHTR). However, the alloy has weakness against oxidation above 650^{0}C and corrosive environment of Pb-Bi eutectic is also highly detrimental for it. It is seen that, deposited coating works as a protective layer on TZM and resists oxidation and corrosion of the alloy at elevated temperatures in Pb-Bi eutectic.

Introduction

The TZM alloy having composition, 99.4% Mo, 0.5% Ti, 0.08% Zr, 0.02% C (wt%) is one of the most favourable alloy as material for Compact high temperature reactor (CHTR) [1]. This alloy has several attributes suitable for high temperature structural applications including high melting temperature (>2600^{0}C), high creep strength at elevated temperature and good corrosion compatibility with many molten metal and alloys. However the alloy, when exposed to elevated temperature is highly susceptible to oxidation making it thermodynamically unstable and chemically vulnerable. Mo, a transition metal plays a crucial role in influencing the oxidation behaviour of TZM alloy. Studies have indicated that between 450^{0}C and 650^{0}C Mo forms MoO_2 and other sub-oxides (MoO_z) where $2 < Z < 3$ and above 650^{0}C, it forms MoO_3 which is highly volatile. As a result, the alloy loses structural integrity and its important mechanical properties are drastically affected due to generation of MoO_3. Hence, in recent past, efforts have been made to develop silicide and aluminide type of coatings over TZM to serve as anti-corrosive and oxidation resistant coating. However, whether these coatings can successfully fulfil all the requirements is yet to be established [2]. Diamond like carbon SiO_x (DLC-SiO_x) is another coating which is chemically inert and gives excellent protection against corrosion & oxidation. It also provides high electrical insulation [3]. All these known benefits of DLC-SiOx make it a good choice for deposition on TZM alloy. However, till date there are no available reports of DLC-SiO_x deposition on TZM alloy. Plasma enhanced chemical vapour deposition (PECVD) is one of the most popular techniques to deposit thin films for various applications. We have used PECVD technique to deposit a protective coating of DLC-SiO_x on TZM alloy and tested its resistance against oxidation and corrosion.

Deposition of DLC-SiO_x on TZM

A 13.56 MHz capacitively coupled PECVD system was used SiOx film on TZM. For this purpose a mixture of Ar and CH_4 at 1:2 ratio was used with controlled flow of hexa- methyl di-siloxane (HMDSO) to generate plasma at 90 Watts power. All the depositions were done for 60 minutes duration on TZM samples. Fig. 1 shows the schematic of the system.

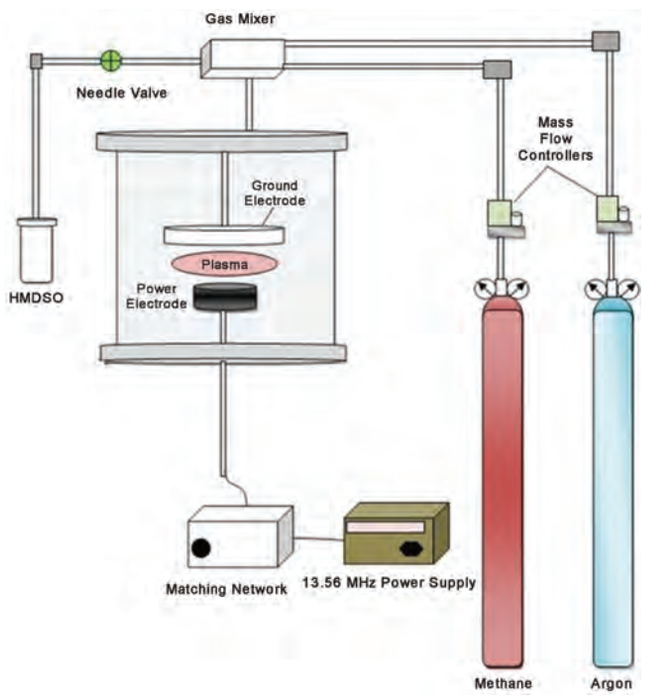

Fig. 1: Schematic of the PECVD system

Characterization of DLC-SiOx film

Deposited films were subjected to surface characterization studies by scanning electron microscopy (SEM), energy dispersive electron spectroscopy (EDS), Raman spectroscopy and property evaluation studies by hardness measurement, oxidation and corrosion tests. Fig. 2(a) shows SEM image of both the uncoated and DLC-SiO_x coated substrate. From the figure, it is observed that after coating, rough unpolished TZM surface has become considerably smoother but it retained some non-uniformity as undulations and voids are

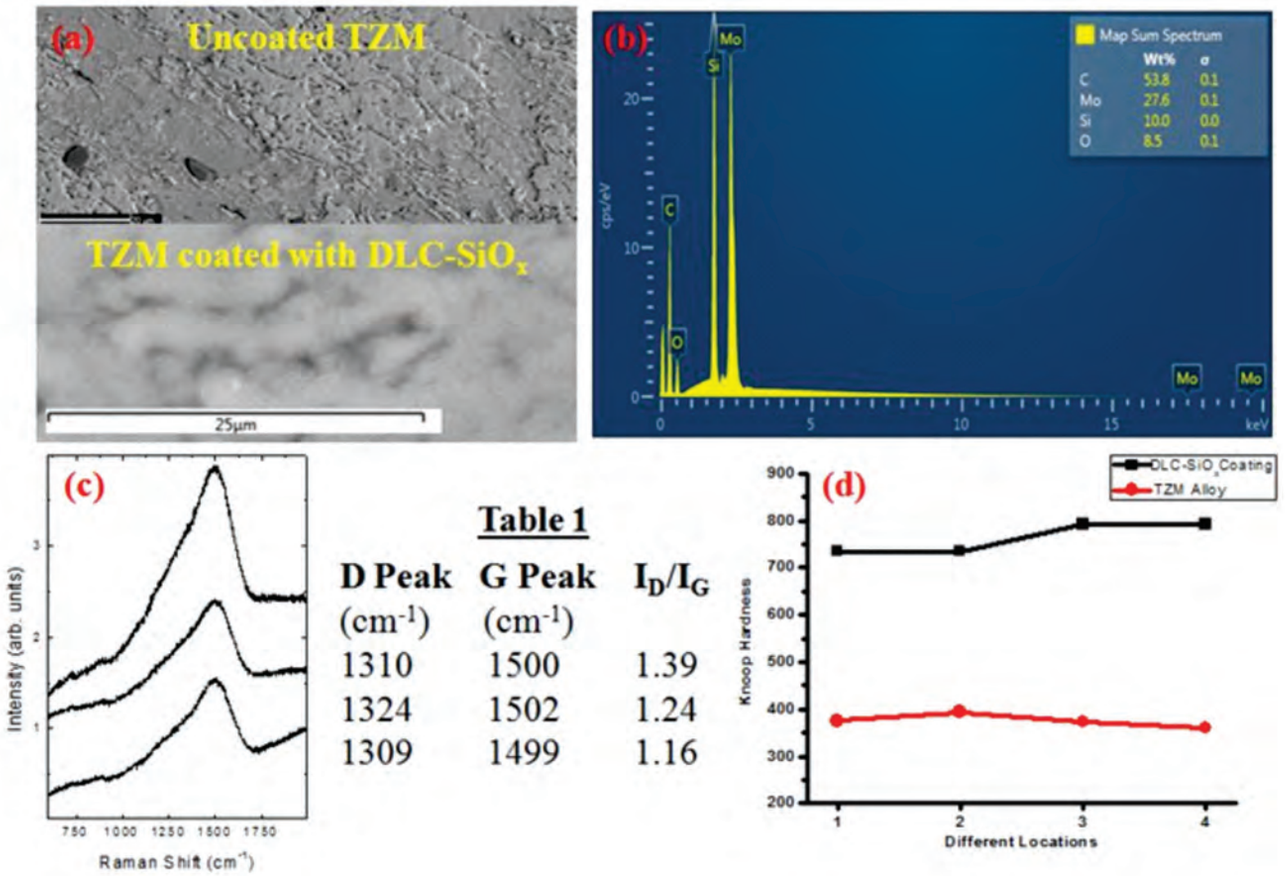

Fig. 2: (a) SEM image of uncoated and coated TZM alloy, (b) EDS spectrum, (c) Raman spectrum of DLC-SiO_x film deposited on TZM alloy, table 1 shows D, G peak positions and I_D/I_G ratios, (d) hardness measurement on DLC-SiO_x coating and TZM alloy at four different locations

seen in the image. This is solely because of the substrate effect which itself was very rough with machining and other track marks present before deposition. The rough surface of the substrate could be a major cause for such non-uniform deposition. However, coating was found to be dense with a thickness of around 1.6 micrometers. Fig. 2(b) shows the EDS spectrum taken on the sample, where inset box shows the percentage of different elements present, C being the most abundant element present followed by Mo which came predominantly from the substrate. Presence of Si and O confirmed that DLC-SiO_x film was formed on TZM surface. Fig. 2(c) shows Raman spectroscopic data of DLC-SiO_x coating taken at three different locations of the film while important parameters like D band, G band and I_D/I_G ratio are presented in Table 1. Presence of D and G band confirms formation of DLC-SiO_x film on TZM alloy [3]. Fig. 2(d) shows measured hardness data taken at four different locations on DLC-SiO_x film as well as on the substrate surface. From the graph, it is seen that hardness almost doubled due to deposition of DLC-SiO_x coating on the substrate surface.

It has to be mentioned that all these characterization techniques are complimentary to each other. Here, EDS characterization proves that carbon-SiO_x based coating has been deposited on the TZM surface while Raman spectroscopic analysis reveals that this coating is essentially an amorphous carbon film, its diamond like nature is indicated by hardness measurement.

Oxidation & corrosion studies: These two studies are most important from application point of view as our basic aim was to protect the TZM alloy from oxidation and corrosion by developing DLC-SiO_x as a protective coating over it.

For oxidation studies, two similar types of TZM samples were initially prepared. One of these samples was coated on both the sides with DLC-SiO_x while the other was left uncoated. Weight of both coated and uncoated sample was measured prior to this study. Subsequently, these two samples were placed inside a muffle furnace and isothermally heated at 800^0C for 150 min. It is well known that TZM alloy containing >99.4% Mo undergoes severe oxidation during heating above 650^0C in air due to vaporization of highly volatile MoO_3 [4]. Figure 3(a) shows the image taken during oxidation which shows vapour being released from the TZM surface due to oxidation. The oxidation profiles of both uncoated and coated TZM alloy samples are presented in Fig. 3(b). From the figure, it is seen that uncoated sample registered ~ 39% weight reduction while for the coated sample the recorded weight loss was only ~ 5.5%.

Corrosion resistance of the coating was tested by dipping both coated and uncoated TZM samples weighing 8 gm each in 900 gm Pb-Bi eutectic molten bath at 800^0C for 3 hrs. However, as the rate of weight change of the samples inside Pb-Bi eutectic is very sluggish, a sizeable weight change could not be recorded in this case. However, there was remarkable

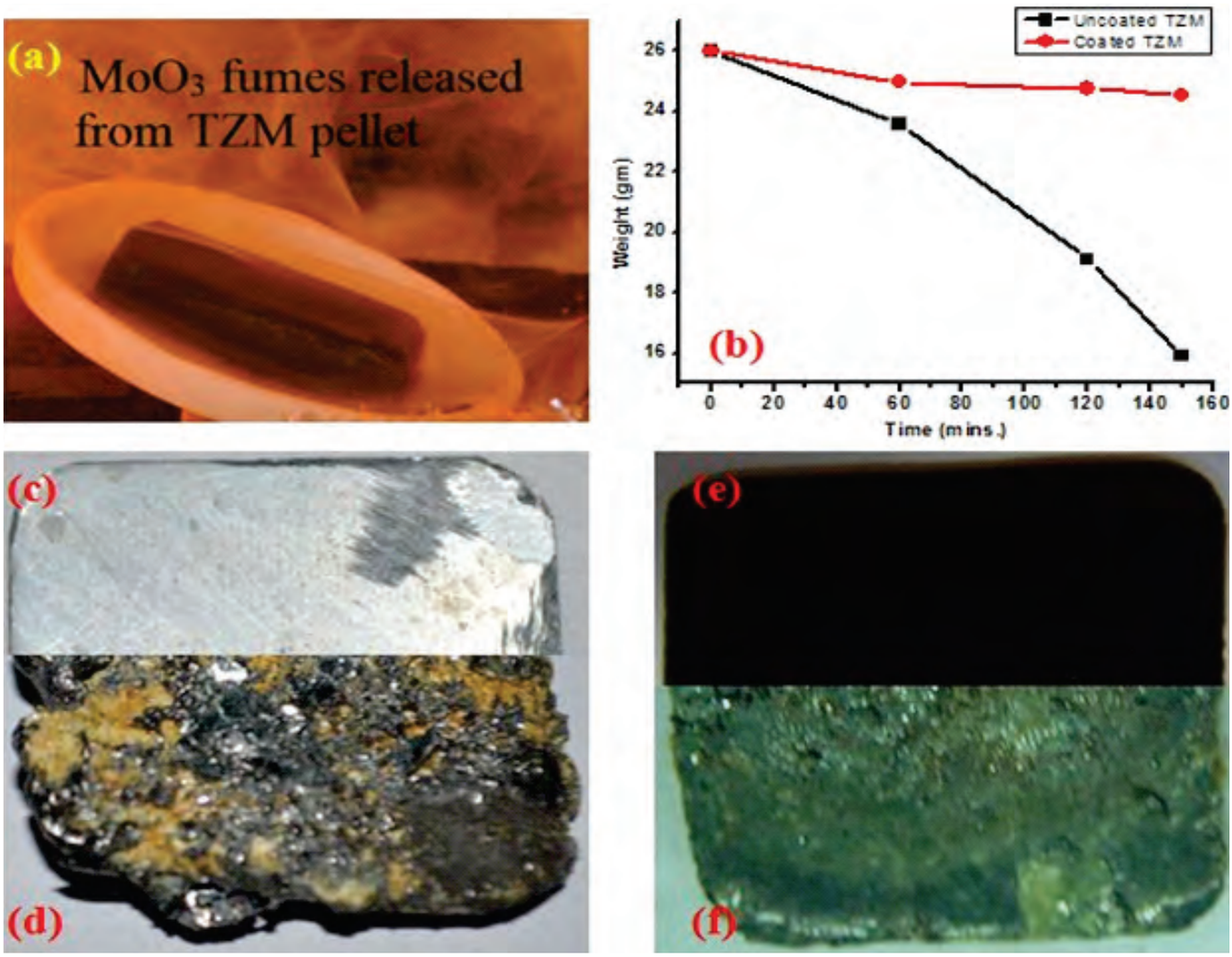

Fig. 3: (a) MoO_3 fumes being released from TZM pellet during oxidation, (b) results from the oxidation studies of coated and uncoated TZM alloy, condition of uncoated TZM alloy (c) before & (d) after corrosion test, condition of DLC-SiO_x coated TZM alloy (d) before & (e) after corrosion test

change in the appearance of the uncoated corroded sample compared to the coated one. Figs. 3(c) and 3(d) show condition of the uncoated TZM sample respectively before and after corrosion experiments. From the figures, it is clear that the uncoated TZM is heavily corroded in comparison to the coated sample inside corrosive Pb-Bi eutectic bath. Figs. 3(e) and 3(f) show corrosion test results on DLC-SiO_x coated TZM sample. Comparing figs. 3(d) and 3(f), it is clearly seen that uncoated TZM is heavily corroded in comparison to the coated sample inside corrosive Pb-Bi eutectic bath.

These preliminary results presented here suggest that DLC-SiO_x has potential to serve as an oxidation and corrosion resistant, protective coating, suitable for use in CHTR.

Acknowledgements

Authors acknowledge the role of Dr. Madangopal Krishnan (Materials Group, BARC) for his keen interest in the present work, and Dr. Kulwant Singh (MSD, BARC) for his support in carrying out hardness measurements as part of this work.

Reference

1. Compact High Temperature Reactor, I.V. Dulera, A. Basak, P.P. Kelkar, R.K. Sinha, Sixteenth Annual Conference of Indian Nuclear Society, INSAC-2005, Mumbai, November, 2005.
2. Studies on the development of TZM alloy by alumina thermic co reduction process and formation of protective coating over the alloy by plasma spray technique, S.P. Chakraborty, Int. Journal of Refractory Metals and Hard Materials 29 (2011) 623–630.
3. SiO_x containing diamond like carbon coatings: Effect of substrate bias during deposition, S.A. Barve, S.S. Chopade, R. Kar , N. Chand, M.N. Deo, A. Biswas, N.N. Patel, G.M. Rao, D.S. Patil, S. Sinha, Diamond & Related Materials 71 (2017) 63–72.
4. Development of silicide coating over molybdenum based refractory alloy and its characterization, S.P. Chakraborty, S. Banerjee, I.G. Sharma, A.K. Suri, J. of Nucl. Mater. 403 (2010) 152-159.

हल्दी में पाये जाने वाले पादपपोषी 'कुरक्यूमिन' के विविध औषधीय गुण

डॉ. (श्रीमती) के. इंदिरा प्रियदर्शिनी
रासायनिकी प्रभाग

भारतीय समाज में हल्दी (Curcuma Longa) को प्राचीन काल से ही बहुत महत्वपूर्ण स्थान दिया गया है। यह अदरक परिवार का एक बारहमासी पौधा है, जो दक्षिण एशिया के उष्णकटिबंधीय और उपोष्णकटिबंधीय क्षेत्रों में उगाया जाता है। भारत का स्थान विश्व में हल्दी के सबसे बड़े उत्पादकों में से एक है। हजारों सालों से हल्दी को परंपरागत भारतीय और चीनी दवाओं में गठिया, मस्तिष्क, खुले घावों, उदर संबंधी विकारों, पेट फूलना, खसरा, अल्सर, पीलिया, त्वचा और आंखों के संक्रमण जैसी बीमारियों का इलाज करने के लिए प्रयोग किया जाता है। आहार के रूप में भारतीय व्यंजनों में हल्दी को नियमित रूप से एक मसाले के रूप में तथा रंगीन अभिकर्मक के रूप में भी प्रयोग किया जाता है। हल्दी का गाढा पीला रंग मुख्य रूप से पॉलीफेनॉल की उपस्थिति के कारण होता है, जिसे 'कुरक्यूमिनोइड' कहा जाता है। पैदावार के स्रोत और मिट्टी के गुणों के आधार पर हल्दी में कुरक्यूमिनोइडों का अंश शुष्क हल्दी के वजन का 2 से 9% तक होता है। कुरक्यूमिनोइड शब्द 'कुरक्यूमिन', 'डिमेथॉक्सीकुरक्यूमिन', 'बिसडिमेथॉक्सी कुरक्यूमिन' तथा 'चक्रीय कुरक्यूमिन' नामक चार यौगिकों के मिश्रण को संदर्भित करता है। कुल कुरक्यूमिनोइडों का लगभग 70% भाग कुरक्यूमिन के रूप में पाया जाता है। इन कुरक्यूमिनोइडों के अलावा हल्दी में टर्मीरॉनों तथा टर्मीरॉल जैसे आवश्यक तेल भी पाये जाते हैं। हल्दी एवं इसके सबसे प्रमुख अवयव कुरक्युमिन दोनों को ही खाद्य पदार्थों में प्रयोग किये जाने को मान्यता दी गई है।

वर्तमान समय में कुरक्यूमिन अत्यधिक शोध किए जाने वाले अणुओं में से एक है, जिसे आधुनिक वैज्ञानिकों द्वारा अक्सर 'इलाजी-जीरा' या 'Cure-Cumin' के रूप में संदर्भित किया जाता है। पिछले तीन से चार दशकों में किये गये पूर्ववर्ती चिकित्सीय अध्ययनों ने कई बीमारियों के खिलाफ कुरक्यूमिन की चिकित्सीय क्षमता स्थापित की है। चिकित्सालयीन अध्ययन में रोगियों द्वारा कुरक्यूमिन को सुरक्षित तथा सुचारु रूप से सहन करते हुए पाया गया है। मनुष्यों द्वारा कुरक्यूमिन के 8 ग्राम प्रति दिन मात्रा तक के सेवन को सुरक्षित माना गया है । मधुमेह, आंत्र-सूजन रोग और गठिया जैसे रोगों के खिलाफ इसकी प्रभावकारिता को चिकित्सालयों में सिद्ध किया जा चुका है। कुरक्यूमिन और हल्दी पर आधारित 'न्यूट्रास्यूटिकल फॉर्मूलेशन' बहुत लोकप्रिय हो रहे हैं। पुरानी बीमारियों से ग्रस्त एवं उनका इलाज कराते हुए मरीजों तथा स्वस्थ लोगों, इन दोनों ही प्रकार के व्यक्तियों के लिए इनके प्रयोग की सिफारिश की जा रही है।

यदि हम इतिहास पर नजर डालें तो कुरक्यूमिन के पृथकन एवं रासायनिक गुणों पर पहली वैज्ञानिक रिपोर्ट वर्ष 1815 में तैयार की गयी थी और इसके आण्विक सूत्र और रासायनिक संरचना को 1910 में प्रकाशित किया गया था। प्रयोगशाला में इसका पहला संश्लेषण 1913 में प्रदर्शित किया गया था और इसके बाद इसके जैव-संश्लेषण (biosynthesis) को समझा गया था। व्यावसायिक तौर पर हल्दी से कुरक्यूमिन को प्राप्त करने हेतु इथेनॉल के साथ विलायक निष्कर्षण (solvent extraction) एवं स्तंभ वर्णक्रमिकी (column chromatography) क्रियाएं संपन्न की जाती हैं।

प्राचीन औषधीय दस्तावेजों के अलावा, 1937 में मानव रोग के इलाज के लिए कुरक्यूमिन पर पहला वैज्ञानिक दस्तावेज बनाया गया था, जिसमें लम्बी अवधि से कॉलिसिस्टिटिस (cholecystitis) रोग से ग्रसित कम से कम 67 रोगियों का इलाज किया गया था। इस इलाज में कुरकूनट (curcunat) का प्रयोग किया गया था, जिसे कुरक्यूमिन के समान ही माना जाता है। कालांतर में वर्ष 1949 में कुरक्यूमिन की जीवाणुरोधी (antibacterial) गतिविधि स्थापित की गई। तब से और 1970 के दशक के बीच तक इसकी जैविक गतिविधियों पर बहुत कम रिपोर्टें उपलब्ध थीं। प्रारंभिक शोध ज्यादातर प्रतिऑक्सीकरक (antioxidant) और जीवाणुरोधी गतिविधियों पर केंद्रित थी। वर्ष 1987 में पहली बार मानव प्रतिभागियों में कैंसररोधी रिपोर्ट जारी हुई थी। इसके बाद, कृंतक

(rodent) के प्रतिदर्श (model) में कई उत्साहजनक परिणामों के साथ कुरक्यूमिन ने पूरे विश्व के शोधकर्ताओं का ध्यान अपनी ओर आकर्षित किया, ताकि उसे एक शक्तिशाली कैंसररोधी (anticancer) औषधि के रूप में विकसित किया जा सके। स्कोपस (SCOPUS) की खोज रिकॉर्ड के अनुसार, जुलाई 2018 तक 'कुरक्यूमिन' शीर्षक के साथ 21000 से अधिक लेख दर्ज किए गए हैं, जिसमें 1000 समीक्षाएं और लगभग 140 चिकित्सीय परीक्षण शामिल हैं। इनमें से आधे से अधिक सामग्री पिछले पांच वर्षों में प्रकाशित हुई है।

रासायनिक रूप से, कुरक्यूमिन एक डाईएराइल्हेप्टानॉइड (d iarylheptanoid) है, जिसमें तीन महत्वपूर्ण क्रियाशील घटक (moieties) पाये जाते हैं। इसमें दो ओ- मेथॉक्सी फेनोलिक समूह (o-methoxy phenolic) होते हैं, जो एक ऐसे हेप्टानोइड लिंकर से जुड़े होते हैं, जिसमें एक एनोन तथा 1,3- डाईकीटोन समूह संयुग्मित होते हैं (चित्र 1) ।

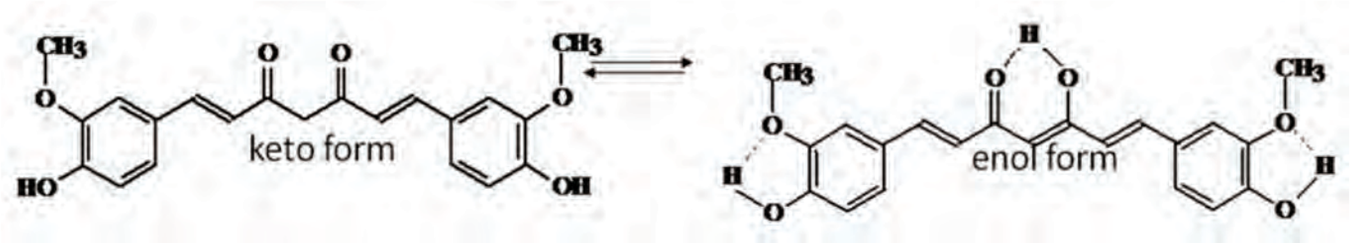

चित्र 1: कुरक्यूमिन की क़ीटो-एनोल संरचनाएं

कुरक्यूमिन के ओ- मेथॉक्सी फेनोलिक- ओएच समूह (o-methoxy phenolic-OH group) मुख्य रूप से ऑक्सीकारी तनाव (oxidative stress) के दौरान उत्पादित मुक्त मूलकों (free radicals) को निष्क्रिय कर देता है तथा इसे श्रृंखला तोड़ने वाले प्रतिऑक्सीकरक के रूप में विटामिन- ई से भी बेहतर माना गया है। कुरक्यूमिन प्रोटीन, लिपिड और डीएनए जैसे कई जैव- अणुओं से बंध बनाता है। ट्रांसक्रिप्शन कारक, सूजन अणु, काइनेज, ट्यूबुलिन, एमिलॉयड- बीटा एग्रीग्रेट, आसंजकी अणुओं (adhesion molecules) , विकास कारक (ग्रोथ फैक्टर) , रिसेप्टर प्रोटीन, प्रोटोफिलामेंट्स, प्रिऑन प्रोटीन जैसे प्रोटीन इत्यादि कुरक्यूमिन के साथ क्रियाएं करते हैं। कुरक्यूमिन धातुओं और धात्वीय- प्रोटीनों से मिलकर सहसंयोजक क्रियाओं के माध्यम से उनके साथ बंध बनाता है। कुरक्यूमिन के साथ एल्युमिनियम(+3) एवं अन्य धातु आयनों के बंधन की भूमिका को अल्जाइमर रोग की रोगजनकता को रोकने में शामिल कारकों में से एक मुख्य कारक माना जा रहा है।

मुख्यत: आंतों में कुरक्यूमिन के अपेक्षाकृत कम अवशोषण और यकृत में तेजी से चयापचय (metabolism) के कारण इसकी बेहद कम जैव- उपलब्धता एक औषधि के रूप में कुरक्यूमिन के विकास में आडे आती है। इसकी जैव- उपलब्धता (bioavailability) बढ़ाने के लिए, शोधकर्ताओं ने कई आदर्श एवं अभिनव फॉर्मूलेशन विकसित किए हैं। इस दिशा में लिपोसोम, नैनोइमल्शंस, पेजाइलेशंस, पॉलिमर, हाइड्रोजेल, साइक्लोडेक्स्ट्रिन्स, पाइपरिन- संयुक्त, स्वर्ण (gold) और मीजोपोरस सिलिका पर आश्रित नैनो कंजूगेट्स और कुरक्यूमिन- लौह ऑक्साइड चुंबकीय नैनोकणों आदि के नाम अत्यधिक महत्वपूर्ण हैं। इनके सुनियोजन से कुरक्यूमिन की जैव उपलब्धता में एक महत्वपूर्ण सुधार आने के साथ- साथ कुरक्यूमिन की इन- विवो बायोएक्टिविटी (शरीर के भीतर होने वाली जैवसक्रियता) भी प्रदर्शित की जा चुकी है। इनमें से अधिकतर फॉर्मूलों को जलीय बफर माध्यम में बनाया जा सकता है।

कृंतक मॉडल में कई पुरानी रोगजनक स्थितियों/बीमारियों तथा विशेषकर कैंसर के खिलाफ कुरक्यूमिन की चिकित्सीय प्रभाविकता का मूल्यांकन किया गया है। ऑक्सीकारी तनाव और सूजन के विरुद्ध कुरक्यूमिन के प्रयोग को एक महत्वपूर्ण उपाय के रूप में पहचाना गया है। इसलिए कई पुरानी बीमारियों के निराकरण हेतु कुरक्यूमिन का उपयोग करने के लिए व्यापक अनुसंधान कार्य शुरू किया गया है। इनमें आंत्र- सूजन (inflammatory bowel) रोग, गठिया (rheumatoid arthritis), मधुमेह, न्यूरोडिजनरेटिव बीमारियां, सोरायसिस, हृदय रोग, एलर्जी, अस्थमा, ब्रोंकाइटिस, गुर्दे की बीमारियां, मोटापा, स्क्लेरोडर्मा, विटिलिगो, पेप्टिक घाव , पिलोरी संक्रमण और नेत्र संबंधी विकार शामिल हैं। चूहों के प्रतिदर्शों (models) में चूहों के शरीर में कुरक्यूमिन प्रविष्ट कराने से त्वचा, पेट, डुओडेनम, कोलन, यकृत, फेफड़े, और स्तन के कैंसर की कार्सिनोजेनेसिस (आरंभ, वृद्धि और फैलाव) प्रक्रिया

के सभी तीन चरण प्रभावित होते हुए पाये गये है। न्यूड माउस में किये गये अध्ययनों के परिणामों से यह भी पता चला है कि कुरक्यूमिन मानव स्तन कैंसर की रोगव्याप्ति (metastasis) को रोकता है।

पूर्व चिकित्सीय अध्ययनों में कैंसर सहित अनेकों दीर्घकालिक (chronic) बीमारियों के विरुद्ध एक चिकित्सकीय अभिकर्मक के रूप में कुरक्यूमिन की उल्लेखनीय सफलता ने चिकित्सकों को मानवों में कई नये नैदानिक परीक्षण करने के लिए प्रेरित किया है। संपूर्ण विश्व में कुरक्यूमिन / हल्दी के निष्कर्षों (एक्स्ट्रैक्ट्स) के साथ किये गये लगभग 141 चिकित्सीय परीक्षणों को एक खोज इंजन (www.clinicaltrials.gov) में वर्णित किया गया है। कुरक्यूमिन ने नैदानिक परीक्षणों में कोलोरेक्टल कैंसर, एबरैंट क्रिप्ट फोसाई, फैमीलियल एडेनोमैटस पॉलीपोसिस (FAP), अग्नाशयी कैंसर मल्टीपिल माइलोमा, हेपेटोसेल्युलर कार्सिनोमा, गैस्ट्रिक कैंसर, और कोलन कैंसर जैसे मानव कैंसरों की एक श्रृंखला के खिलाफ रसोसंरक्षी (chemopreventive) और उपचारात्मक प्रभाव (therapeutic effect) प्रदर्शित किया है। कई अन्य बीमारियों के निराकरण हेतु बहुत से नैदानिक परीक्षण चलाए जा रहे हैं और कई नये परीक्षण शुरू भी किए जा रहे हैं।

संपूर्ण विश्व में कुरक्यूमिन पर होने वाला अनुसंधान कार्य लगातार तेजी से बढ़ रहा है। ऐसा माना जाता है कि जिस तरह से कुरक्यूमिन संबंधी विषयों पर कार्य करने को एक वैज्ञानिक पर्व मनाने जैसा स्थान दिया गया है, उस तरह का स्थान किसी अन्य वनस्पति अणु को नहीं मिला है। भाभा परमाणु अनुसंधान केंद्र में विकसित किये गये कुरक्यूमिन उत्पादों की कुछ प्रतिनिधि तस्वीरें नीचे प्रदर्शित की गयी हैं

Turbovita CURe-Sol ND Gel-CURe

हल्दी पर आधारित स्वास्थ्य रक्षा उत्पादों (healthc are products) की बढ़ती क्षमता को ध्यान में रखते हुए, बीएआरसी में न्यूट्रास्यूटिकल (Turbovita) और जैव-उपलब्ध (bioavailable) कुरक्यूमिन फॉर्मूलेशन के उत्पादन के लिए प्रौद्योगिकियों का विकास किया गया है।इन प्रौद्योगिकियों को क्रमशः मेसर्स वीणा इंडस्ट्रीज, नागपुर और मेसर्स अकाई फ्लेवर्स एंड अरोमैटिक्स, कोच्चि को स्थानांतरित कर दिया गया है । संभावित औषधीय अनुप्रयोगों के रूप में विकसित किए गए अन्य कुरक्यूमिन उत्पादों में नाक में डालने वाले नेसल ड्रॉप, हाइड्रोजेल पैच और हाइड्रोक्सीएपेटाइट नैनोपार्टिकिल्स शामिल हैं।

अभिस्वीकृति

लेखिका अपने वर्ग के सभी सदस्यों, पुराने तथा नये छात्रों और उन सभी सहयोगियों के प्रति धन्यवाद ज्ञापित करती हैं, जिन्होंने हल्दी पर आधारित इस शोधकार्य में अपना बहुमूल्य योगदान दिया है।

संदर्भ:

1. S. C. Gupta, S. Patchva, B. B. Aggarwal, Therapeutic Roles of Curcumin: Lessons Learned from Clinical Trials-The AAPS Journal, 2013 (15) 195-219

2. A. Goel, A. B.Kunnumakkara, B. B.Aggarwal, Curcumin as "Curecumin": From kitchen to clinic.Biochem Pharma. 2008 (75) 787-809

3. K. I. Priyadarsini, Chemistry of Curucmin: from extraction to therapeutic agent. Molecules, 2014 (19) 20091-20112

4. A Kunwar, K I Priyadarsini, Curcumin and Its Role in Chronic Diseases.Adv Exp Med Biol. 2016 (928) 1-25

Process for ^{99}Tc Removal from Intermediate Level Waste of Reprocessing Origin by in-situ formed Corrosion Product of Mild Steel Wool

A. Ananthanarayanan, S. Pahan, D. Banerjee, Pallavi. P. S., M. A. Rao, S. A. Khot
A. Joseph, J. G. Shah and K. Agarwal
Nuclear Recycle Group
T. P. Valsala
Nuclear Recycle Board, Tarapur

A novel process has been developed for removal of Technetium (^{99}Tc) from intermediate liquid waste (ILW) by making use of in-situ formed corrosion products of mild steel. The process has been demonstrated with the actual ILW at NRB, Tarapur. A healthy decontamination factor of 2000 was also demonstrated in the process.

Introduction

Technetium (^{99}Tc) arising from spent fuel reprocessing is a major radiation concern owing to a combination of high thermal fission yield (6%), long half life (2.13×10^5 y), high environmental mobility in oxidized pertechnate form, combined with radioactivity as a β – emitter [1]. Further, ^{99}Tc presents a challenge to conventional high temperature vitrification in a borosilicate glass matrix owing to its volatility at glass synthesis temperatures.

Thus, efforts are underway to capture and sequestrate ^{99}Tc using ion exchange resins (elutable and non-elutable), crown ethers or capture in mineral phases [2, 3]. Indeed, it is known that ^{99}Tc can be sequestrated into various mineral phases including perovskites, rutile, sodalite, trevorite etc [2]. However, the preparation of most of these phases requires high temperature conditions with specialized equipment such as hot isostatic pressing (HIP).

Efforts to utilize goethite/magnetite to capture ^{99}Tc from Sanford Low Activity Waste (LAW) were carried out on bench scale by co-precipitating goethite in the LAW solutions. While Tc capture using goethite was demonstrated in these studies, the ferrihydrite precursor for goethite formation was synthesized ex-situ under anoxic conditions [4]. Synthesis, and particularly storage, of ferrihydrite is challenging due to its instability and its conversion to Fe_3O_4 upon exposure to air oxygen [4]. It has also been demonstrated that ex-situ synthesized Fe_3O_4 does not show Tc uptake.

It is clear from the literature that mineralization of Tc in Fe-oxides/oxyhydroxides is well known. Indeed, such take-up has been the subject of several papers and reports listed in the references [1 – 3]. Also, well known is that mild steel can corrode in aqueous environment to produce iron oxides/oxy-hydroxide phases. In the process developed, we exploit corrosion of mild steel to produce the iron oxide/oxy-hydroxide phases required for Tc sequestration, while avoiding ex-situ synthesis of ferrihydrite under demanding anoxic conditions [5].

This paper highlights the process development studies and the results of ^{99}Tc removal with actual Intermediate Level Waste (ILW).

Experimental Techniques

The experimental set-up used for Tc removal studies is presented in Fig. 1.

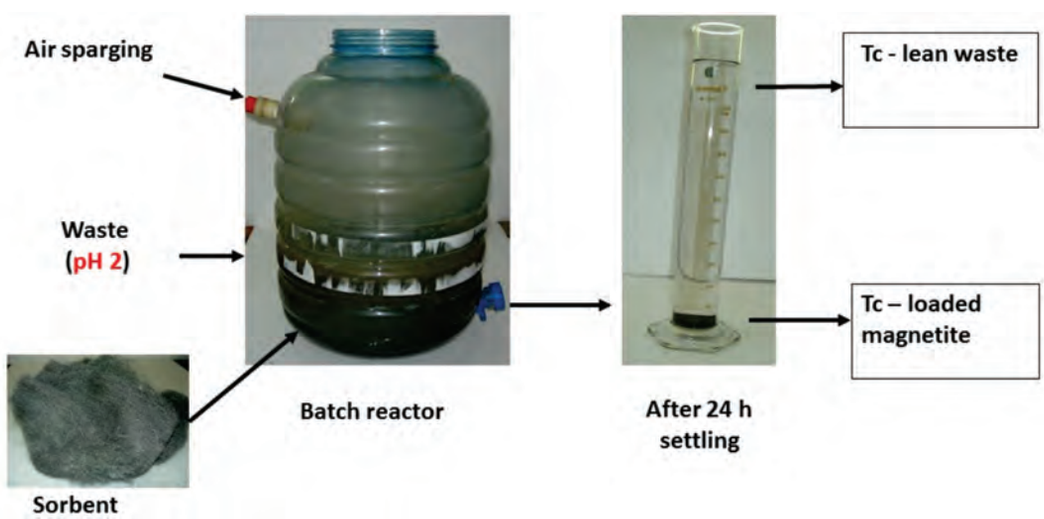

Fig. 1: Lab scale experimental set-up for Tc removal from ILW

The lab scale studies consist of a batch reactor containing MS wool, into which the waste was introduced (V/m = 100). Continuous air bubbling was provided for nearly four hours, and thereafter the solution was left standing overnight, Subsequently, the supernatant was analyzed radiometrically for Tc. Process optimization with respect to V/m ratio, effect of starting pH and effect of anions and nitrates in the ILW were studied and the results are used to arrive at optimum process conditions for Tc removal.

Scale -up studies were then carried out at HIRUP, BARC with simulated waste solutions on a 25 lit. scale using ^{99m}Tc milked from a moly-cow sourced from BRIT, Mumbai. Finally, the process was demonstrated on a 40 lit. scale at NRB Tarapur.

Results and Discussions

In the present process, corrosion of mild steel results in the formation of corrosion products, which then pick up ^{99}Tc from the ILW solution. Therefore, it is necessary to optimize process conditions for in-situ formation of corrosion product and Tc trapping. One of the main process conditions is the pH of the starting solution. Fig. 2 shows the effect of different starting pH on Tc removal performance.

In the case of waste with a pH of 2, an over 99.6% removal of Technetium was observed within the first 2 hours of initiation. During corrosion, release of Fe^{2+} ions from the surface of the corroding steel leads to a concomitant release of OH^- ions which cause an increase in the solution pH from 2 to 6 resulting in the formation of a reddish-brown corrosion product that settles at the bottom. Notably, most of the original activity of the ILW is concentrated in this phase. Since the corrosion product settles to the bottom, separation becomes quite simple.

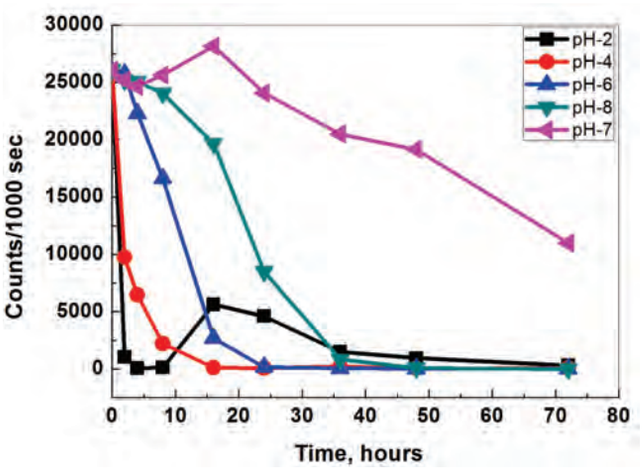

Fig. 2: Tc removal profile as a function of time during corrosion of Ms wool using ILW of varying initial pH, each cases v/m 100 and batch size of 50 mL was used, ^{99}Tc with total counts of ~ 25,000 per ml per 100 seconds of ILW

Similar inactive studies were carried out to generate mineral phases for X-ray Powder Diffraction (XRD) analyses. From these studies, the dominant mineral phase is found to be Goethite (α – FeOOH). It has been shown in the literature that three Tc (IV) can replace four Fe (III) in Goethite (FeOOH), while creating one Fe (III) vacancy as depicted in Figure 3.The Tc(IV) is formed from Tc(VII) by reduction due to Fe(II) according to the following reac tion:

$$Tc\ (VII) + 3\ Fe\ (II) \rightarrow 3\ Fe\ (III) + Tc\ (IV)$$

Further, process parameters such as the V/m ratio, were also optimized on lab scale. It was found that the process is effective over a wide V/m range from 10 to 1000. As expected, process kinetics is significantly accelerated using lower V/m. However, low V/m also results in a larger volume of secondary wastes. On the other hand, a higher V/m ratio reduces secondary waste volume at the expense of slower process kinetics, which is inadequate for plant scale treatment of large waste volumes. Therefore, a V/m of 100 has been selected for further processes.

Bench scale trials at 25 lit. scale using ^{99m}Tc were carried out with various simulated waste solutions containing differing concentrations of $NaNO_3$. One study was also carried out with sea water spiked with ^{99m}Tc to simulate accidental scenario. In all the cases, excellent Tc removal was observed, confirming the efficacy of the process.

A process flow chart based upon above results has been finalized and is presented in Fig. 4.

A demonstration trial has been conducted at 40 lit. scale with actual ILW in NRB, Tarapur. ILW as generated is alkaline in nature, therefore pre-treatment by addition of HNO_3 was carried out to adjust pH to 2. About 400 g MS wool was used in

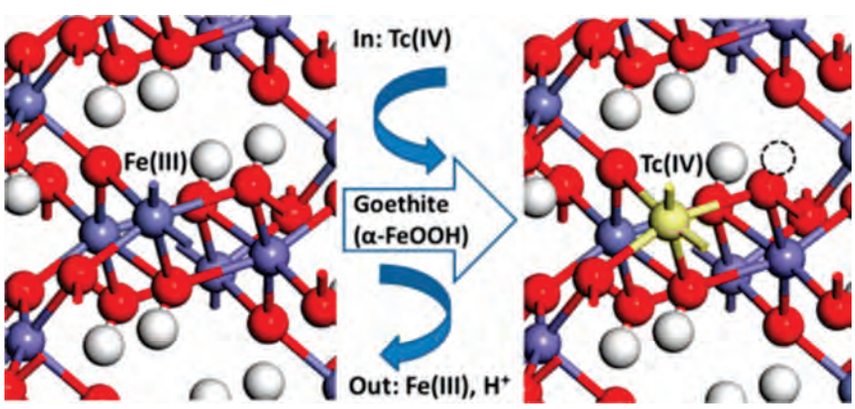

Fig. 3: Possible mechanism for Technetium uptake into the crystal structure of Goethite [1]

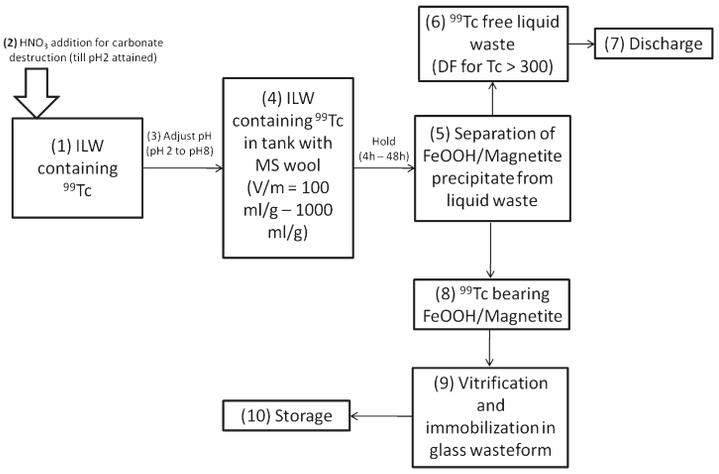

Fig. 4: Process flowsheet for Tc removal from ILW using *in-situ* formed corrosion product of MS wool

Table 2: Radiochemical composition (mCi.l^{-1}) of TRIX effluent (after pH adjustment) used in this study

pH	Gross β	^{99}Tc	^{106}Ru	^{125}Sb	^{137}Cs
2.5 ± 0.5	1.1×10^{-1}	1.1×10^{-1}	1.7×10^{-3}	1.6×10^{-3}	2.4×10^{-2}

Table 3: Decontamination of TRIX effluent using MS wool

Expt No	Time (Hr)	pH	DF				
			Gross β	^{99}Tc	^{106}Ru	^{125}Sb	^{137}Cs
1	3	5.6	4	700	5	3	4
	25	7.0	3	1700	6	15	1
2	3	5.7	8	640	4	3	2
	21	9.3	6	990	8	16	2

Radiochemical composition of the waste is shown in Table 2. The system was agitated continuously by air bubbling, at a flow rate of ~ 1 lpm, for 6 h, and left standing overnight. Samples were withdrawn at periodic intervals for radiochemical analysis. In the second experiment, same MS wool from the previous run was used. The objective of this experiment was to ensure the efficacy of MS wool in repeated experiments, in addition to verification of reproducibility of the results. Results of these experiments are summarized in Table 3.

It is evident from Table 3 that Tc DF of about 1700 was obtained during the first trial and the same MS wool is effective for the second experiment. Laboratory results show that the same wool can be used for more than five cycles. It is noteworthy that this process is useful for removal of ^{106}Ru and ^{125}Sb also, which are major activity contributors to LLW after ^{99}Tc and ^{137}Cs removal. This process generates a small volume of secondary waste, typically in the order of magnitude which is smaller than the conventional processes.

The sludge is amenable to vitrification in suitably optimized glass matrices having a reducing melt environment. In such glasses, Tc retention approaching 70% is presently possible, compared to less than 20% upon direct vitrification of Tc bearing streams in conventional borosilicate glasses.

Conclusions

Tc removal by in-situ formed corrosion product of mild steel wool is an effective method to remove Tc from low and intermediate level wastes. The process generates low volume of secondary sludge, which can be immobilized in a suitable glass matrix. Further R&D is being pursued to process corrosion products and used MS wool into suitable wasteforms.

References

1. F. N. Smith, C. D. Taylor, W. Um and A. A. Kruger, Technetium Incorporation into Goethite (α-FeOOH): An Atomic-Scale Investigation, Environ. Sci. Technol., 2015, 49 (22), 13699–13707.
2. W. Um, H. Chang, J. P. Icenhower, W. W. Lukens, R. J. Serne, N. P. Quafoku, J. H. Westsik Jr., E. C. Buck and S. C. Smith, Immobilization of 99-Technetium (VII) by Fe(II)-Goethite and Limited Reoxidation, Environ. Sci. Technol., 2011, 45 (11), 4904–4913.
3. W. Um, G. Wang, H. B. Jung and R. A. Peterson, Technitium removal using Tc-Goethite coprecipitation, Pacific Northwest National Laboratory Report, 2013, Report Number PNNL-22967; EMSP-RPT-017,
4. R. M. Cornell and U. Schwertmann, The Iron Oxides; Structure, Properties, Reactions, Occurrences and Uses, 2nd Ed., Wiley VCH, 2003.
5. J. G. Shah, S. Pahan and A. Ananthanarayanan, A process for the removal of ^{99}Tc from liquid intermediate level waste of spent fuel reprocessing, PCT Application No. PCT/IN2017/050170.

Development and Demonstration of Vacuum Distillation Process for Recovery of Pure TBP and n-Dodecane from Simulated Organic Liquid Waste

K. K. Haldar and K.V. Ravi
Nuclear Recycle Board, Mumbai
M. M. Malusare and Sanjay Kumar
Nuclear Recycle Board, Tarapur

A mixture of Tri-butyl phosphate (TBP) and n-Dodecane used in nuclear fuel reprocessing plants have limited life because of formation of degradation compounds due to irradiation and chemical attack, leading to generation of spent solvent as radioactive organic Liquid Waste (OLW). To meet the objective of waste minimisation in high throughput plants, it is vital to develop a technology to recover and reuse of solvents from organic waste Vacuum Distillation is envisaged as an effective method for removal of these degradation compounds and recovery of pure TBP & n-Dodecane from the organic waste. Careful design of Vacuum distillation system is very crucial as TBP is not highly volatile, a thermo-sensitive compound at elevated temperatures and having very low concentrations of variety of impurities in organic waste that need to be removed.

A plant scale vacuum distillation demonstration facility has been developed, designed and installed at TWMP, NRB, BARC, Tarapur. Successful trials have been carried out with simulated organic waste with recovery of significant portion of high purity TBP and n-Dodecane. The developed distillation system has an assured potential to become a standard and efficient treatment system in every radioactive organic liquid waste management plants in India.

Introduction

Nuclear fuel reprocessing plants use mixture of 30% TBP and 70% n-Dodecane (diluent) as solvent in PUREX process for extraction of heavy metals. This solvent after repeated use gets degraded mainly due to irradiation and chemical attack. This spent solvent is discarded which contains degradation products such as Di-butyl Phosphate (DBP), High Molecular weight Phosphate(HMP), Mono-Butyl Phosphate (MBP) and various diluent degradation products(DDP) e.g. Nitro, Nitriso compounds, carboxylic acid, alcohol along with radioactivity. In present reprocessing plants, the spent solvent is regenerated by scrubbing with sodium carbonate by which most of the radioactivity associated with DBP is removed. However, residual activity due to other degradation products cannot be removed. These degradation products progressively accumulate in the solvent with repeated recycling and their removal from the solvent is not well addressed. Vacuum Distillation process is a most suitable process for Recovery of pure organics from spent OLW.

With an aim to recover the solvents from the organic waste to reduce the radiological and chemical impact on environment, and to reuse of the recovered pure organics to cut down the operating cost of the reprocessing plants, a vacuum distillation system has been developed after intensive literature survey1,2,3, lab studies, detailed process design and equipment selection. Based on the detailed design, a complete plant scale system has been fabricated, installed and commissioned at Tarapur site for demonstration trials. The developed Vacuum distillation has broadly two sections-1) Evaporation in ATFE for removing major portion of HMP impurity and 2) Batch distillation with rectification in distillation column for recovering pure n-Dodecane and TBP as distillate cuts. During the trials with simulated waste, an effective recovery of TBP and n-Dodecane with purity greater than 99.9% was achieved. The quality of recovered organics is at par with fresh organic being used in reprocessing plants.

Process Description

Vacuum distillation plant is developed as per the process flow scheme shown in Figure-1. Organic waste is received in OLW receipt tank and subjected to washing by 0.5 M sodium carbonate to remove most of the DBP. After washing, organic waste is fed in continuous mode to Agitated Thin Film Evaporator-1 (ATFE-1) section, which is maintained at high vacuum and low temperature. LP steam is used for heating in evaporators. The vapours generated are condensed in a condensers utilizing chilled water. The condensate from ATFE-1 becomes free from major portion of high boiling impurities which remains as residue in the bottom of ATFE-1. Thereafter, a batch of organic condensate collected is transferred to kettle of batch distillation section comprising of Agitated Thin Film Evaporator-2 (ATFE-2) acting as a reboiler, distillation column with rectification section, condenser, reflux drum, etc. High vacuum and low temperature are maintained in ATFE-2. Vapours from ATFE-2 are fed to distillation column, which is operated to recover various distillate cuts like (i) n-Dodecane cut, (ii) impurities (DDP) cut and (iii) TBP cuts, from top of the column by adjusting temperature at ATFE-2. HMP and DBP-rich impurities are retained at bottom of kettle. The purified TBP and n-Dodecane are stored in separate vessels. An alkaline

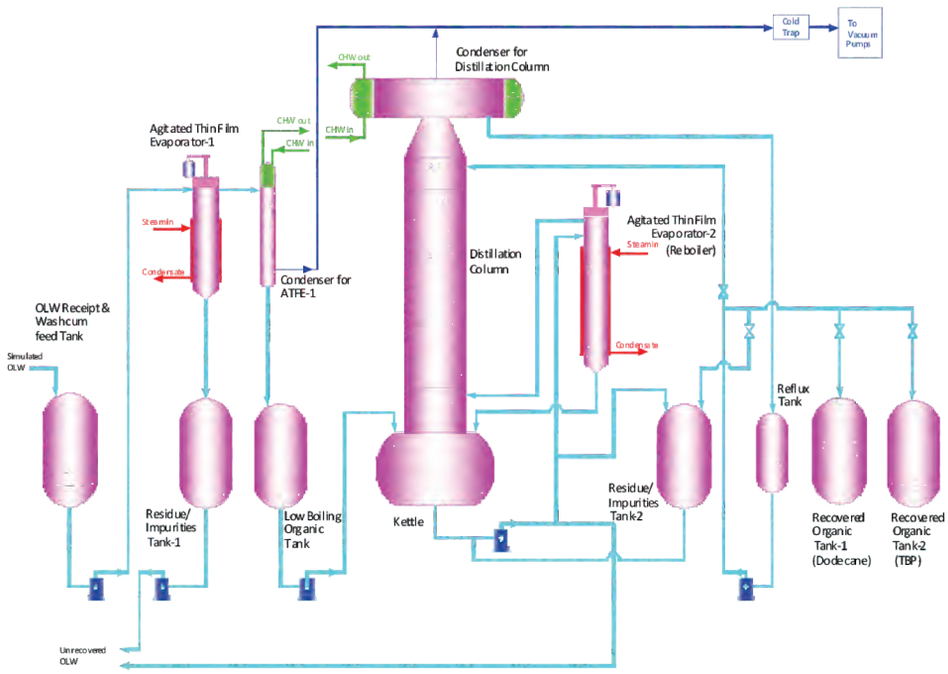

Fig.1: Process Flow Diagram

wash is also provided to the recovered organic to eliminate traces of Di-Butyl Phosphoric acid which could be carried along by the TBP vapours.

For inactive trial runs in this plant, simulated organic waste was used. Simulated organic waste was prepared by equilibrating mixture of 30% TBP & 70% Dodecane with 4M Nitric Acid solution and irradiating the mixture by using gamma source in a radiation field of 1 X 105 R/hr. The irradiation duration was fixed to match the extent of degradation of simulated waste with actual organic waste.

The composition of simulated OLW & plant OLW are as follows:

Equipment Selection

As the TBP is not highly volatile and it is a thermo-sensitive compound, this distillation is carried out at low pressure and temperature by using two stage vacuum pump. To minimize the residence time of the fluid during evaporation in the heated zones, ATFE-1 & ATFE-2 are used. Vapours from ATFEs are condensed in shell and tube type condensers. For purification of TBP & Dodecane, a packed bed distillation column with very low pressure drop and high efficiency is used. 3-D view of the plant is shown in Fig.-2 and photographs of major equipment of this plant are shown in Figure-3 & 4. Alkaline washing tanks are provided for removal of DBP impurities at beginning and at the end of the process cycle.

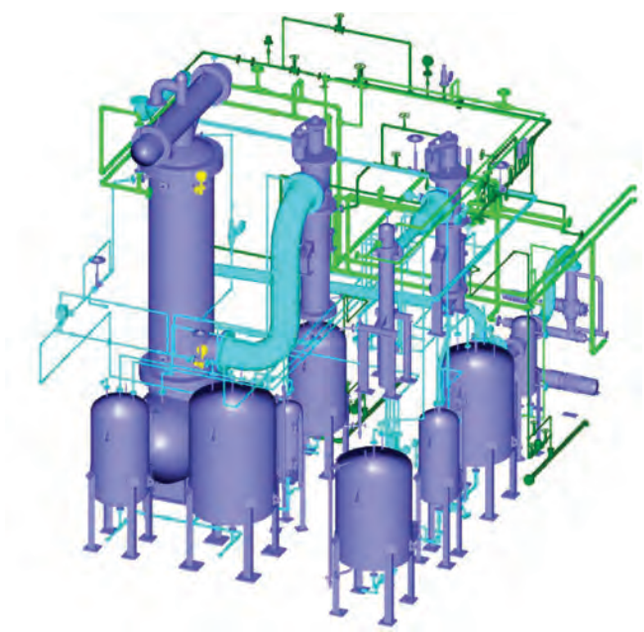

Fig. 2: 3D Plant Model

Mechanical design of process equipment is carried out conforming to ASME Section VIII, Div.1. Material of Construction of all major equipment and associated piping is austenitic stainless steel grade 304L. Instrumentation and Control system has been adapted for monitoring and controlling of process parameters like level, temperature, pressure and flow. Sizing of each equipment & piping has been

Table 1: Composition of simulated OLW & plant OLW

Description	Dodecane	TBP	DDP	HMP	DBP
	Wt%	Wt%	Wt%	Wt%	Wt%
Simulated OLW	65.51%	32.54%	0.90%	0.31%	0.74%
Plant OLW	66.27%	32.57%	0.30%	0.25%	0.62%

Fig.3: Equipment of VDS

arrived for system design capacity of 40 LPH (32 KGPH) feed rate of organic waste.

Laboratory Scale Studies

For design of distillation column, it is imperative to know vapour-liquid equilibrium (VLE) behaviour of TBP and n-Dodecane with respect to major impurities present in organic waste. Various laboratory experiments were conducted at different temperatures and concentrations of TBP, n-Dodecane and impurities. Typical lab results are given below:

These results were used for design of distillation column.

Plant Scale Demonstration Trial Results

The trial runs were carried out with simulated organic waste of about 500 litres (400 kg). After initial carbonate wash, simulated organic waste was fed to ATFE-1. Residue collected at bottom of ATFE-1 operation was maintained at 5-10%. The rest condensed top organics from ATFE-1 operation was transferred to Kettle of batch distillation column. Distillation column was operated in batch mode with rectification in packed bed by giving reflux at varying reflux ratios for different product cuts. Several trial runs were carried out with varying process parameters and samples of recovered n-Dodecane and TBP cuts were analysed by Gas Chromatographer at NRB/NRG Laboratories. The results are tabulated below:

a) Gas Chromatography test results:

Table-5: Gas Chromatography test results

Table 2: Typical normalized VLE behaviour of Dodecane w.r.t. TBP

Temperature	Dodecane		TBP	
^{0}C	% in liquid	% in vapour	% in liquid	% in vapour
75	45.69	91.88	54.31	8.12
90	50.58	95.68	49.42	4.32

Table 3: Typical normalized VLE behaviour of n-Dodecane w.r.t. DDP

Temperature	Dodecane		DDP	
^{0}C	% in liquid	% in vapour	% in liquid	% in vapour
72	99.824	99.945	0.176	0.055
80	99.804	99.874	0.196	0.126

Table 4: Typical VLE behavior of TBP w.r.t. HMP

Temperature	TBP		HMP	
^{0}C	% in liquid	% in vapour	% in liquid	% in vapour
75	49.8	8.1	0.682	0.000
90	47.0	4.3	0.306	0.000

These results were used for design of distillation column.

Table-5: Gas Chromatography test results

DESCRIPTION (STREAMS)	RECOVERY		TBP PURITY	n-DODECANE PURITY	TECH. SPECS. PURITY FOR FRESH ORGANICS
	RECOVERED VOLUME	% RECOVERY			
RECOVERED DODECANE	310 litres (233 kg)	85%	-	99.97%	98%
RECOVERED TBP	40 litres (39 kg)	30%	99.9%	-	99%

b) Uranium Loading & Stripping Test:

Recovered n-Dodecane & TBP was mixed in the ratio of 70:30 and tested for Uranium loading & stripping at reprocessing plant laboratory. The result shows that extent of uranium extraction is 100% and uranium stripped is 99.63%. Thus, U-retention is much less than the minimum required for recycle.

c) Pu retention Test:

Recovered n-Dodecane & TBP was mixed in the ratio of 70:30 and tested for Pu retention test at reprocessing plant laboratory. The extent of Pu retained in organic phase is negligible.

Based on the above test results, Reprocessing Plant Laboratories certified that the quality of vacuum distilled TBP & n-Dodecane is at par with fresh TBP & n-Dodecane.

Conclusion

The plant scale Vacuum Distillation System was successfully developed, designed, fabricated, installed and operated to demonstrate the recovery of Dodecane (85% by volume) with purity of 99.97% and TBP (30% volume) with purity of 99.9% from simulated OLW. The recovered organics quality is at par with fresh organics as certified by reprocessing plant laboratories and meets the specification for reuse in reprocessing plant. The recovery volume of 68.5% of pure solvent from degraded solvent has been achieved and volume of simulated OLW is reduced to 31.5% only. Further trial runs are planned to increase the recovery percentage by adjusting the process parameters.

Acknowledgement

Authors acknowledge the support extended by TWMP, PREFRE-II lab. and PP lab in the form of logistics and laboratory services, as part of this study.

References

1 P. Pradel, G. Dalverny & J-P.Moulin. "The Organic Waste Treatment in UP3-La Hague". International Conference on Nuclear Fuel Reprocessing and Waste Management, (1991).

2 S.C. Tripathi, A. Ramanujam, K.K. Gupta, P. Bindu. "Studies on the identification of harmful radiolytic products of 30% TBP-dodecane-HNO3 by gas-chromatography- II. Formation of molecular weight organophosphates". Sep. Sci. Technol. 36, (2001).

3 F. Sicilio, T. H. Goodgame, B. Wilkins, Jr. "Purification of irradiated tributyl phosphate in kerosene type diluent by distillation". Nuclear Science Engineering, (1961).

Abbreviations

TBP: Tri-n-butyl phosphate

DBP: Di-butyl phosphate

MBP: Mono butyl phosphate

DDP: Diluent (n-dodecane) degradation products

HMP: High molecular weight phosphates

ATFE: Agitated thin film evaporator

OLW: Organic liquid waste

RP: Reprocessing plant

Seventeenth Training Course on Crane and Forklift Operations Organised by BARC Safety Council at BARC Facilities, Kalpakkam

Seventeenth Training Course on Crane and Forklift operations organised by BARC Safety Council at BARC Facilities, KalpakkamThe Material Handling Equipment (MHE) committee of the Conventional & Fire Safety Review Committee (CFSRC) of the BARC Safety Council (BSC) regularly conducts training courses on 'Crane Operation' and 'Crane maintenance', with an aim to impart general awareness on safe practices in crane operation, regulatory requirements, fault diagnosis & maintenance of EOT cranes and industrial safety for the staff of DAE.

The 17th training course on 'Crane and Forklift Operations' was conducted at Kalpakkam during December 4-7, 2017, for Technicians and Scientific Assistants of BARC Facilities, Kalpakkam, and RMP, Mysore. This was the second course conducted at Kalpakkam by the BSC.

The training course was inaugurated on December 4, 2017 at KARP Lecture Hall.

Shri B. Shreekumar, General Manager, INRP(K), welcomed the dignitaries and the participants at the function. Shri S.Rajendran, Member-Secretary, MHE Committee briefed the role of MHE Committee for procurement, periodical inspection, testing & certification of MHE in his introductory remarks. Shri K. Jayarajan, Chairman, BSC delivering the inaugural address stated the importance of training to the operators to achieve accident-free environment.

Shri Kailash Agarwal, Chairman, MHE Committee and Associate Director, NRG, delivered the keynote address. He briefed the operations carried out through MHE in nuclear plants and stated that operator training and refresher course are essential for safe operation of the nuclear plant, as the materials handled in nuclear plants are hazardous. Further, he emphasized that forklift operation was included in this course for the first time to teach aspects of theory and practice on safe operation of forklift. Shri Ananthakrishnan, MHE Zonal Coordinator, Kalpakkam, proposed the vote of thanks.

Inaugural function: Release of Training Course Manual
from left to right - Shri S. Rajendran, Shri K. Jayarajan, Shri Kailash Agarwal and Shri B. Shreekumar

Central Complex at BARC

Edited & Published by:
Scientific Information Resource Division
Bhabha Atomic Research Centre, Trombay, Mumbai 400 085, India
BARC Newsletter is also available at URL:http://www.barc.gov.in